Numer. Math. Theor. Meth. Appl.
doi: 10.4208/nmtma.OA-2023-0088

Vol. **17**, No. 1, pp. 1-36
February 2024

Multidomain Hybrid Direct DG and Central Difference Methods for Viscous Terms in Hyperbolic-Parabolic Equations

Weixiong Yuan, Tiegang Liu, Bin Zhang, Kui Cao and Kun Wang*

LMIB and School of Mathematical Sciences, Beihang University, Beijing 100191, China

Received 23 July 2023; Accepted (in revised version) 16 October 2023

Abstract. A class of multidomain hybrid methods of direct discontinuous Galerkin (DDG) methods and central difference (CD) schemes for the viscous terms is proposed in this paper. Both conservative and nonconservative coupling modes are discussed. To treat the shock wave, the nonconservative coupling mode automatically switch to conservative coupling mode to preserve the conservative property when discontinuities pass through the artificial interface. To maintain the accuracy of the hybrid methods, the Lagrange interpolation polynomials and their derivatives are reconstructed to handle the coupling cells in the DDG subdomain, while the values of ghost points for the CD subdomain are calculated by the approximate polynomials from the DDG methods. The linear stabilities of these methods are demonstrated in detail through von-Neumann analysis. The multidomain hybrid DDG and CD methods are then extended to one- and two-dimensional hyperbolic-parabolic equations. Numerical results validate that the multidomain hybrid methods are high-order accurate in the smooth regions, robust for viscous shock simulations and capable to save computational cost.

AMS subject classifications: 65M60, 65M06, 65M99, 35L65, 35K20

Key words: Direct discontinuous Galerkin, central difference schemes, multidomain hybrid methods, viscous terms, hyperbolic-parabolic equations.

1. Introduction

To accurately predict the engineering problems and fundamental flow physics, high-order methods, such as discontinuous Galerkin methods (DG) [9–13,26] and weighted essentially non-oscillatory schemes (WENO) [19,20,31,33,34,38,48], have attracted more interest recently with the lower numerical dissipation. Except for those methods,

*Corresponding author. *Email address:* `wangkun@buaa.edu.cn` (K. Wang)

high-order hybrid methods have been developed to combine the advantages of each individual method.

Luo *et al.* [24] presented a reconstruction-based discontinuous Galerkin (RDG (P1P2)) method, where the quadratic polynomial solution (P2) is obtained from the underlying linear polynomial (P1) discontinuous Galerkin solution using a least-squares method. Zhang *et al.* [42–45] proposed a hybrid DG/FV scheme, where the lower-order derivatives of a piecewise polynomial solution are computed locally in a cell by the DG methods and the higher-order derivatives are reconstructed by the known lower-order derivatives. Later, Zhao *et al.* [46] optimized the reconstruction strategy for DG/FV methods by a hierarchical reconstruction strategy, where the cell average and its derivatives were reconstructed by WENO reconstruction. Zhu *et al.* [47] and Guo *et al.* [16] developed a hybrid WCNS-CPR scheme for the efficient supersonic simulations, where WCNS is adopted to capture shocks while the smooth area is calculated by CPR. Maltsev *et al.* [25] developed a hybrid DG/FV schemes, in which the key ingredient is a switch between DG method and FV method based on the CWENOZ scheme. Based on the computational domain decomposition, Cheng *et al.* [4, 6, 7] proposed the multidomain hybrid RKDG and WENO methods for solving the hyperbolic conservation laws, which combined the advantages of high efficiency of the WENO schemes and easy treatment of the complex geometries easily from the DG methods. Later, Zhang *et al.* [41] analyzed the linear stabilities of the conservative multidomain hybrid methods and introduced two ways of healing the stable problems. Moreover, Wang *et al.* [37] proposed a novel high-order FD scheme based on DG boundary treatment and no more than two layers were needed for the complex boundary treatments. Up to date, the multidomain hybrid methods have been proposed to treat the inviscid terms in the compressible inviscid flow problems. To take the advantages of the method in solving compressible viscous flow problems, we extend the multidomain hybrid methods to handle the viscous terms and then apply the methods to solve hyperbolic-parabolic equations.

Central difference schemes are often used to discretize the viscous terms in the finite difference methods. Compared to the formulas used in [15, 49], Shen *et al.* [27–30] proposed a set of conservative fourth- and sixth-order central difference schemes for compressible flows with variable viscosity coefficient, which has the stencil width matching that of the fifth- and seventh-order WENO schemes and maintains the compactness of the WENO schemes. It is conservative and highly efficient but difficult to handle the complex geometries just as finite difference WENO schemes. In the DG methods, taking a simple arithmetic mean of the solution derivatives from the left and right is inconsistent [32]. A number of numerical methods have been proposed in the literature to address this issue. Among those methods, the direct discontinuous Galerkin methods [22, 23] are based on the direct weak formulation for solving the parabolic equations. The viscous numerical flux constructed in the DDG methods is consistent and conservative and no auxiliary variable required during the calculation. Later, Cheng *et al.* [5, 8, 40] extended the DDG methods to discretize the viscous and heat fluxes in the Navier-Stokes equations. The DDG methods are simple, conserva-

tive, and easy to handle complex geometries but take high computational costs as DG methods.

In this paper, we propose multidomain hybrid DDG and CD methods (DDG/CD) for the viscous terms in hyperbolic-parabolic equations based on the domain decomposition and give the linear stability analysis of these methods. For the consideration of computational cost, the hybrid method of a third-order DDG method with a fourth-order CD scheme for the parabolic equations will be presented to illustrate the idea. Firstly, we decompose the computational domain into the CD and DDG subdomains. At the artificial interfaces, both DDG and CD numerical fluxes can be constructed. Therefore, there can be two types of hybrid methods. One is the conservative hybrid methods with the same one flux at the artificial interface, and the other is the nonconservative hybrid methods with their own fluxes. To handle shock wave, the nonconservative multidomain hybrid methods switch to conservative hybrid methods to preserve the conservative property when discontinuities pass through the artificial interface. We will show that the nonconservative hybrid methods can preserve high order in the smooth regions, while the conservative hybrid methods are only of first order but with the correct position of the shock wave preserved. The linear stability analysis shows that both the conservative and nonconservative methods are linearly stable. Combining with the multidomain hybrid DG and WENO methods for the inviscid terms, we will extend the multidomain hybrid methods to the hyperbolic-parabolic equations. A total variation bounded (TVB) shock wave detector is employed to detect the possible discontinuities. Finally, the multidomain hybrid methods are extended to two-dimensional Navier-Stokes equations. Numerical results illustrate that the multidomain hybrid methods are high-order accurate in the smooth regions, robust for viscous shock simulations and capable of saving computational cost.

The rest of this paper is arranged as follows. In Section 2, we give a brief introduction to the DDG methods and CD schemes. In Section 3, the multidomain hybrid DDG/CD methods for the viscous terms are proposed. The stability and the accuracy of the hybrid DDG/CD methods are presented in Section 4. In Section 5, we extend the multidomain hybrid methods to the hyperbolic-parabolic equations. Then we confirm the effectiveness of these methods through various numerical tests in Section 6. Finally, concluding remarks and suggestions for future work are given in Section 7.

2. Brief introduction to the discretization of viscous terms

2.1. Governing equations

To better illustrate the idea of the multidomain hybrid methods for the viscous terms, we consider the following one-dimensional scalar parabolic equation:

$$\begin{cases} u_t = h(u, u_x)_x, & x \in [a, b], \\ u(x, 0) = u_0(x), & t \in [0, T]. \end{cases} \tag{2.1}$$

The computation domain $[a, b]$ can be divided into N grids where $a = x_{1/2} < x_{3/2} < \cdots < x_{N+1/2} = b$. Also, the j-th cell is defined as $I_j = (x_{j-1/2}, x_{j+1/2}), j = 1, 2, \ldots, N$, and the j-th cell size is $\Delta x_j = x_{j+1/2} - x_{j-1/2}$.

2.2. The direct discontinuous Galerkin method

For direct discontinuous Galerkin methods [22, 23], the numerical solution $u_h(x, t)$ is defined in the finite-dimensional space $U_h^k = \{p : p|_{I_j} \in P^k(I_j)\}$, where $P^k(I_j)$ is a polynomial with the degree at most k, are the basis functions defined in the cell I_j. The Legendre orthogonal basis functions are adopted here, and can be listed as follows:

$$\varphi_0^j = 1.0, \quad \varphi_1^j = 2\frac{x - x_j}{\Delta x}, \quad \varphi_2^j = 4\left(\frac{x - x_j}{\Delta x}\right)^2 - \frac{1}{3}, \ldots . \tag{2.2}$$

Defining the degree of the freedom $u_j^l(t)$ in the cell I_j as

$$u_j^l(t) = \int_{I_j} u(x,t)\varphi_l^j(x)dx \left(\int_{I_j} \left(\varphi_l^j(x)\right)^2 dx\right)^{-1}, \tag{2.3}$$

the numerical solution can be expressed as

$$u_h(x,t) = \sum_{l=0}^{k} u_j^l(t)\varphi_l^j(x). \tag{2.4}$$

Multiplying Eq. (2.1) by the test function $v(x)$, and integrating by parts in I_j, we can obtain the weak form formulation

$$\int_{I_j} u_t v dx = \widehat{h}(u, u_x)_{j+1/2} v_{j+1/2} - \widehat{h}(u, u_x)_{j-1/2} v_{j-1/2} - \int_{I_j} h(u, u_x) v_x dx. \tag{2.5}$$

The viscous numerical fluxes $\widehat{h}(u, u_x)_{j\pm 1/2}$ can be defined by the DDG methods

$$\begin{aligned} &\widehat{h}(u, u_x) = \beta_0 \frac{[b(u)]}{\Delta x} + \overline{b(u)_x} + \beta_1 \Delta x [b(u)_{xx}], \\ &[u] = u^+ - u^-, \quad \overline{u} = \frac{u^+ + u^-}{2}, \\ &h = a(u)u_x, \qquad b(u) = \int^u a(s)ds. \end{aligned} \tag{2.6}$$

Here, $\beta_0 = 2$ and $\beta_1 = 1/12$ are usually specified. The integral $\int_{I_j} h(u, u_x) v_x dx$ can be either computed exactly or approximated by using suitable numerical quadratures, and we can get the final semi-discrete scheme

$$u_t = L_h(u), \tag{2.7}$$

which is then discretized in time with the third-order accurate strong stability preserving Runge-Kutta method (SSPRK(3,3)) [36].

2.3. The central difference schemes

For the Eq. (2.1), a conservative scheme in the finite difference method can be written as

$$u_t = \frac{\widehat{h}_{j+1/2} - \widehat{h}_{j-1/2}}{\Delta x}, \tag{2.8}$$

where $\widehat{h}_{j\pm 1/2}$ are the viscous numerical fluxes. If the viscous flux h is linear, such as $h(u, u_x) = \mu u_x$, where the viscosity coefficient μ is constant, it is straightforward to do the discretization. However, if the viscosity coefficient is variable as in the compressible flows, the conservative high-order finite difference schemes for the viscous terms are not obvious [27–30].

To obtain the high-order accuracy, the viscous numerical flux $\widehat{h}_{j+1/2}$ needs to be constructed as

$$\widehat{h}_{j+1/2} = \sum_{J=k}^{d} \alpha_J h_J, \tag{2.9}$$

where $J = \ldots, j-1/2, j+1/2, j+3/2, \ldots$ are the boundary points of the cells to be determined and the approximation of the viscous term is given below

$$u_J = \sum_{l=m}^{n} C_l^J u_{j+l}, \quad \frac{\partial u}{\partial x}\Big|_J = \frac{1}{\Delta x} \sum_{l=r}^{s} D_l^J u_{j+l}. \tag{2.10}$$

If a two-dimensional equation is considered and the cross derivatives $\partial u/\partial y|_J$ occur, the cross derivatives are discretized in a dimension by dimension fashion, where

$$\frac{\partial u}{\partial y}\Big|_J = \sum_{l=m}^{n} C_l^J \frac{\partial u}{\partial y}\Big|_{j+l,i}, \quad \frac{\partial u}{\partial y}\Big|_{j,i} = \frac{1}{\Delta y} \sum_{l=p}^{q} C_l^c u_{j,i+l}. \tag{2.11}$$

By ensuring that the approximation of $h(u, u_x)_x|_{x_j}$ is a central difference scheme, we can choose different ranges for (k, d), (m, n), (r, s), (p, q) and coefficients α, C_l^J, D_l^J, C_l^c to obtain desirable order accurate approximation for the viscous terms. Finally, the semi-discrete scheme $u_t = L_h(u)$ can be obtained and then discreted in time by the third-order accurate strong stability preserving Runge-Kutta method (SSPRK(3,3)) [36]. Taking the fourth-order central difference scheme as an example, $(k, d) = (-1, 1)$, $(m, n) = (-2, 1)$, $(r, s) = (-3, 2)$ and $(p, q) = (-2, 2)$ are used, where the coefficients α, C_l^J, D_l^J, C_l^c can be obtained by Taylor's series expansion and are given in Tables 1-4.

Table 1: The coefficients of α.

$\alpha_{j-1/2}$	$\alpha_{j+1/2}$	$\alpha_{j+3/2}$
$-1/24$	$26/24$	$-1/24$

Table 2: The coefficients of C_l^J.

J	C_{-2}^J	C_{-1}^J	C_0^J	C_1^J
$j-1/2$	$5/16$	$15/16$	$-5/16$	$1/16$
$j+1/2$	$-1/16$	$9/16$	$9/16$	$-1/16$
$j+3/2$	$1/16$	$-5/16$	$15/16$	$5/16$

Table 3: The coefficients of D_l^J.

J	D_{-3}^J	D_{-2}^J	D_{-1}^J	D_0^J	D_1^J	D_2^J
$j-1/2$	$71/1920$	$-141/128$	$69/64$	$1/192$	$-3/128$	$3/640$
$j+1/2$	$-3/640$	$25/384$	$-75/64$	$75/64$	$-25/384$	$3/640$
$j+3/2$	$-3/640$	$3/128$	$-1/192$	$-69/64$	$141/128$	$-71/1920$

Table 4: The coefficients of C_l^c.

C_{-2}^c	C_{-1}^c	C_0^c	C_1^c	C_2^c
$1/12$	$-8/12$	0	$8/12$	$-1/12$

3. Multidomain hybrid method for viscous term

In this section, we focus on the implementation of multidomain hybrid methods for the viscous terms in Eq. (2.1). Firstly, we will adopt the following statements. The computational domain computed by a DDG method is called the DDG subdomain, while the domain computed by a central difference scheme is called the central difference subdomain, which can be simplified as the CD subdomain. The computational domain $[a, b]$ is divided into two subdomains as shown in Fig. 1. The left subdomain $[x_{1/2}, x_{J+1/2}]$ is for the DDG methods and the right subdomain $[x_{J+1/2}, x_{N+1/2}]$ is for the central difference schemes, where the artificial interface is located at $x = x_{J+1/2}$. Then we have a semi-discrete form of the multidomain hybrid methods expressed as

$$\begin{cases} \dfrac{d}{dt}u_j = \dfrac{1}{\Delta x_j}\left(\widehat{h}_{j+1/2}^{DDG} - \widehat{h}_{j-1/2}^{DDG}\right), & j = 1, 2, \ldots, J, \\ \dfrac{d}{dt}u_j = \dfrac{1}{\Delta x_j}\left(\widehat{h}_{j+1/2}^{CD} - \widehat{h}_{j-1/2}^{CD}\right), & j = J+1, J+2, \ldots, N, \end{cases} \tag{3.1}$$

where $\widehat{h}_{j+1/2}^{DDG}$ $(j = 0, 1, \ldots, J)$ and $\widehat{h}_{j+1/2}^{CD}$ $(j = J, J+1, \ldots, N)$ are the viscous numerical fluxes in the DDG subdomain and CD subdomain, respectively. Here, u_j represents point values for the CD subdomain and cell average values (zero degree of the freedom) for the DDG subdomain, and the semi-discrete form is not listed out for the higher-order degrees of the freedom of the DDG method.

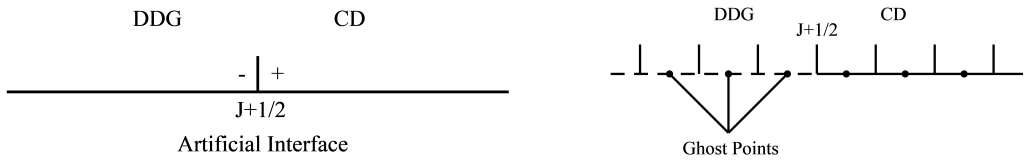

(a) Domain decomposition in one dimension (b) Ghost points for CD subdomain

Figure 1: Multidomain hybrid methods for one-dimensional problems.

At the artificial interface $x = x_{J+1/2}$, two kinds of the viscous numerical fluxes $\widehat{h}^{DDG}_{J+1/2}$ and $\widehat{h}^{CD}_{J+1/2}$ represent the respective viscous fluxes in different subdomains. Now the key point is how to construct the viscous numerical fluxes at the artificial interface, which can result in two different types of the discretization for the multidomain hybrid method. If we take the unique viscous numerical flux at the artificial interface $x_{J+1/2}$, which means $\widehat{h}^{DDG}_{J+1/2} = \widehat{h}^{CD}_{J+1/2}$, we call this conservative multidomain hybrid method. More specifically, the DDG method and CD scheme use the same viscous numerical flux at the artificial interface. Otherwise, if the different viscous numerical fluxes are used at the artificial interface, we refer to this as the nonconservative multidomain hybrid method.

3.1. Nonconservative multidomain hybrid methods for viscous term

In the nonconservative multidomain hybrid method, we need to reconstruct the viscous numerical fluxes for the DDG method and CD scheme at the artificial interface, respectively. Here we use a nonconservative hybrid third-order DDG and fourth-order central difference method to illustrate the procedure. We again use the Fig. 1 as an example where the DDG subdomain is on the left and the CD subdomain is on the right of the artificial interface $x = x_{J+1/2}$. We assume that the grids of both the DDG subdomain and CD subdomain are uniform ($\Delta x_j = \Delta x$) for analysis, but a uniform grid is not required in the DDG subdomain actually in applications.

Case 1. The reconstruction for the CD flux at the artificial interface.

The reconstruction of the viscous numerical flux for the CD subdomain at the artificial interface $x = x_{J+1/2}$ involves two matters. One is the values of the ghost points, as shown in Fig. 1(b), which can be calculated by the DDG methods directly. More specifically, according to the formulas (2.9), we only need the point values u^{CD}_{J-2}, u^{CD}_{J-1}, u^{CD}_{J} at the ghost points x_{J-2}, x_{J-1}, x_J inside the DDG subdomain for the construction of $\widehat{h}^{4thCD}_{J+1/2}$. The other is, if the two-dimensional equations are considered, the values of the ghost points in the boundary regions as shown in Fig. 2(a), which can be obtained from the boundary conditions. In this work, the point values u^{CD}_{J-2}, u^{CD}_{J-1}, u^{CD}_{J} are calculated by the approximate polynomials (2.4) provided from the DDG method, and the reconstruction of the CD viscous numerical flux is then well completed.

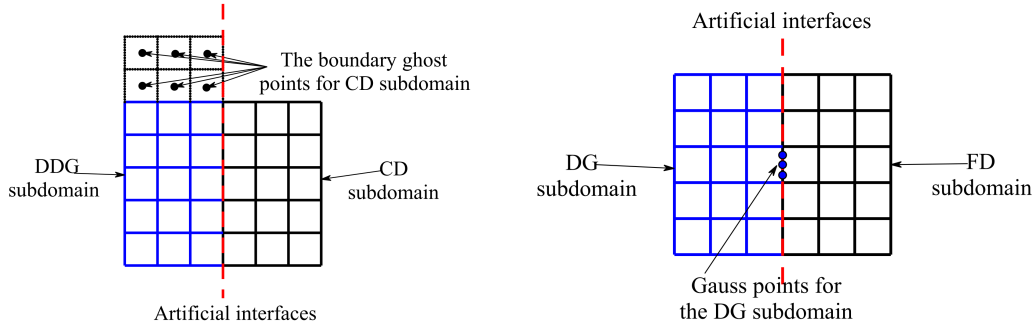

(a) The boundary ghost points for CD subdomain (b) The Gauss points for the DG subdomain

Figure 2: The special points in two-dimensional structure meshes.

Case 2. The reconstruction for the DDG flux at the artificial interface.

Next, we mainly focus on the reconstruction of the viscous numerical flux for the DDG method at the artificial interface $x = x_{J+1/2}$. According to the Eqs. (2.6), not only the function values $b(u)^{\pm}_{J+1/2}$ but also their first and second derivatives are needed in the DDG method. More specifically, the values $u^{\pm}_{J+1/2}$, $u^{\pm}_{x,J+1/2}$, $u^{\pm}_{xx,J+1/2}$ are necessary. For the values $u^{-}_{J+1/2}$, $u^{-}_{x,J+1/2}$, $u^{-}_{xx,J+1/2}$, we can calculate the point values through the formulas

$$\begin{cases} u^{-}_{J+1/2} = u_h(x,t)|_{x_{J+1/2}} = \sum_{l=0}^{k-1} u^l_J(t)\varphi^J_l(x)|_{x_{J+1/2}}, \\ \frac{d}{dx}u^{-}_{J+1/2} = \frac{d}{dx}u_h(x,t)|_{x_{J+1/2}} = \sum_{l=0}^{k-1} u^l_J(t)\frac{d}{dx}\varphi^J_l(x)|_{x_{J+1/2}}, \\ \frac{d^2}{dx^2}u^{-}_{J+1/2} = \frac{d^2}{dx^2}u_h(x,t)|_{x_{J+1/2}} = \sum_{l=0}^{k-1} u^l_J(t)\frac{d^2}{dx^2}\varphi^J_l(x)|_{x_{J+1/2}}. \end{cases} \tag{3.2}$$

However, it is not obvious to compute $u^{+}_{J+1/2}$, $u^{+}_{x,J+1/2}$, $u^{+}_{xx,J+1/2}$ because the CD subdomain can only supply the point values rather than the degrees of freedom u^l_j $(l = 0, 1, 2, \ldots)$, which are needed by the DDG method. We employ the Lagrange interpolation polynomial to calculate these values. For the P^k-based DDG method, we need to use (2k+1) point values to construct the interpolation polynomials in order to compute the values $u^{+}_{J+1/2}$, $u^{+}_{x,J+1/2}$, $u^{+}_{xx,J+1/2}$ for the desirable accuracy. Here we take the third-order DDG method as an example to explain the procedure by the following three steps:

Step 1. As shown in the Eq. (3.3), we use a five point interpolation stencil $S = \{I_{J-1}, I_J, I_{J+1}, I_{J+2}, I_{J+3}\}$ to construct the Lagrange interpolation polynomial $p_5(x)$, which satisfies $p_5(x_k) = u_k (k = J-1, J, \ldots, J+3)$. It is noted that u_{J-1}, u_J are the central point values in the cells I_{J-1}, I_J from the DDG subdomain, which can be

computed by the DDG methods. And the central point values u_{J+1}, u_{J+2}, u_{J+3} can be obtained from the CD schemes directly

$$p_5(x) = \sum_{k=J-1}^{J+3} l_k(x)u(x_k), \quad l_k(x) = \prod_{j=J-1, j\neq k}^{J+3} \frac{x - x_j}{x_k - x_j}. \tag{3.3}$$

Step 2. The corresponding first and second derivative formulas of the function $p_5(x)$ can be calculated directly via the derivative operation. And then, the values of the specific points can be calculated through the formulas

$$\begin{cases} u^+_{J+1/2} = p_5(x_{J+1/2}) \\ = -\dfrac{5}{128}u_{J-1} + \dfrac{15}{32}u_J + \dfrac{45}{64}u_{J+1} - \dfrac{5}{32}u_{J+2} + \dfrac{3}{128}u_{J+3}, \\ \dfrac{d}{dx}u^+_{J+1/2} = \dfrac{d}{dx}p_5(x_{J+1/2}) \\ = \dfrac{1}{24\Delta x}(u_{J-1} - 27u_J + 27u_{J+1} - u_{J+2}), \\ \dfrac{d^2}{dx^2}u^+_{J+1/2} = \dfrac{d^2}{dx^2}p_5(x_{J+1/2}) \\ = \dfrac{1}{24\Delta x^2}(7u_{J-1} + 8u_J - 42u_{J+1} + 32u_{J+2} - 5u_{J+3}). \end{cases} \tag{3.4}$$

Step 3. We can calculate the variable values $b(u_{J+1/2})^+$, $b(u_{J+1/2})^+_x$, $b(u_{J+1/2})^+_{xx}$ based on (2.6) and (3.4). Then, the viscous numerical flux $\widehat{h}^{DDGP2}_{J+1/2}$ can be computed as the final step and the reconstruction for the DDG flux at the artificial interface is accomplished well.

If the solution is smooth enough, we can discretize the equation according to the formulas above and use the nonconservative hybrid method completely. However, if there is a discontinuity near the artificial interface, then it is suitable to choose a unique viscous numerical flux to guarantee correct position of the shock wave, which means the nonconservative hybrid method should automatically switch to the conservative hybrid method.

In this paper, the TVB minmod function is applied as the shock detector to detect the possible discontinuities. The details are listed as following steps:

Step 1. For the coupling cell I_J in the DDG subdomain, the values $u^-_{J+1/2}$, $u^+_{J-1/2}$ can be calculated in the cell I_J directly

$$u^-_{J+1/2} = u_h(x_{J+1/2}, t), \quad u^+_{J-1/2} = u_h(x_{J-1/2}, t).$$

Then, we can calculate the values $\widetilde{u}_J$, $\widetilde{\widetilde{u}}_J$ by the following formulas:

$$\widetilde{u}_J = u^-_{J+1/2} - u^0_J, \quad \widetilde{\widetilde{u}}_J = u^0_J - u^+_{J-1/2}. \tag{3.5}$$

Step 2. For the jump of the cell average of the solution, we can calculate the $\Delta_- u_J = u_J^0 - u_{J-1}^0$, where u_{J-1}^0 and u_J^0 are the zero degree of freedom in cells I_{J-1}, I_J respectively. As for $\Delta_+ u_J$, we can calculate the $\Delta_+ u_J = u_{J+1}^0 - u_J^0$, where u_{J+1}^0 are the zero degree of freedom in cell I_{J+1} from the CD subdomain, which can be taken as the point values u_{J+1} directly.

Step 3. We perform the TVB shock detector at the cell I_J

$$\widetilde{u}_J^{(mod)} = m(\widetilde{u}_J, \Delta_+ u_J, \Delta_- u_J), \quad \widetilde{\widetilde{u}}_J^{(mod)} = m(\widetilde{\widetilde{u}}_J, \Delta_+ u_J, \Delta_- u_J), \tag{3.6}$$

where m is the usual TVB minmod function.

Step 4. If $\widetilde{u}_J^{(mod)} \neq \widetilde{u}_J$ or $\widetilde{\widetilde{u}}_J^{(mod)} \neq \widetilde{\widetilde{u}}_J$, it means that the solution in the cell I_J may be discontinuous and the conservative hybrid methods are applied.

3.2. Conservative multidomain hybrid method for viscous term

According to the Subsection 3.1, two types of the viscous numerical fluxes $\widehat{h}_{J+1/2}^{DDG}$ and $\widehat{h}_{J+1/2}^{CD}$ at the artificial interface $x_{J+1/2}$ are reconstructed, where the values of the numerical fluxes are different generally. If we use the unique viscous flux $\widehat{h}_{J+1/2}^{DDG} = \widehat{h}_{J+1/2}^{CD} = \widehat{h}_{J+1/2}$ at the artificial interface, we can obtain a conservative hybrid method and the semi-discrete form of the equation at the coupling cells I_J, I_{J+1} can be expressed as

$$\begin{cases} \dfrac{d}{dt} u_j = \dfrac{1}{\Delta x_J}\big(\widehat{h}_{J+1/2} - \widehat{h}_{J-1/2}^{DDG}\big), & j = J, \\ \dfrac{d}{dt} u_j = \dfrac{1}{\Delta x_j}\big(\widehat{h}_{J+3/2}^{CD} - \widehat{h}_{J+1/2}\big), & j = J+1. \end{cases} \tag{3.7}$$

The problem is which viscous numerical flux should be chosen for the consideration of stability. In the next section, the detailed proofs of the stability are given, which reveal that both the viscous numerical fluxes are linear stable and admissible.

Now we can summarize the multidomain hybrid methods for the viscous terms.

Algorithm 3.1

1: Decompose the computational domain.
2: Initialize the degrees of freedom for the DDG methods and the point values for the central difference schemes according to the initial conditions.
3: Assign the values of the ghost points for the central difference schemes, and then calculate the viscous numerical flux $\widehat{h}_{j+1/2}^{CD}, j = J, J+1, \ldots, N$ in the CD subdomain.
4: Calculate the viscous numerical flux $\widehat{h}_{j+1/2}^{DDG}, j = 0, 1, \ldots, J-1$ in the DDG subdomain except the artificial interfaces.
5: Use a shock detector to detect the possible discontinuity at the artificial interface: If the coupling cell does not include discontinuity, then the nonconservative hybrid methods are adopted. Otherwise, the conservative hybrid methods are applied with a unique conservative numerical flux at the artificial interface.

6: If the nonconservative hybrid methods are applied at the coupling cells, construct the Lagrange interpolation polynomials for the DDG subdomain, calculate the first and second derivatives needed by the DDG methods, compute viscous numerical flux $\widehat{h}^{DDG}_{J+1/2}$ at the artificial interface.
7: Update the degrees of freedom in the DDG subdomain and the point values in the CD subdomain respectively.
8: Advance to the next moment according to the third-order SSPRK method and repeat the Steps 3-7 until to the given calculation time.

3.3. Time discretization

As for the time discretization, an explicit third-order accurate strong stability preserving Runge-Kutta method (SSPRK(3,3)) [36] is applied with a CFL number equal to the minimum of the CFL numbers of all the subdomains. The third-order SSPRK method is given as follows:

$$\begin{cases} u^{(1)} = u^n + \Delta t L(u^n), \\ u^{(2)} = \dfrac{3}{4}u^n + \dfrac{1}{4}u^{(1)} + \dfrac{1}{4}\Delta t L(u^{(1)}), \\ u^{n+1} = \dfrac{1}{3}u^n + \dfrac{2}{3}u^{(2)} + \dfrac{2}{3}\Delta t L(u^{(2)}). \end{cases} \tag{3.8}$$

4. Theoretical analysis

4.1. Stability analysis

In the following subsections, we will give the linear stability analysis of the conservative multidomain hybrid method for the viscous terms. According to the TVD theorem in [11], for a semi-discrete scheme

$$\frac{d}{dt}u^h = L_h(u^h, t), \tag{4.1}$$

where L_h is the spatial operator. Applying a high order TVD Runge-Kutta method for time iteration, the whole scheme is TVD under a CFL restriction if the spatial operator is TVD. As the third-order accurate strong stability preserving Runge-Kutta method (SSPRK(3,3)) [36] is TVD, it guarantees the stability of the whole scheme if the spatial discretization is stable. Therefore, we only need to consider the stability of the semi-discrete form of space discretization for the hybrid methods.

For the analysis of stability for the conservative multidomain hybrid method of the viscous terms, we will consider the following one dimensional linear diffusion equation:

$$u_t = \mu u_{xx}, \quad (x,t) \in [a,b] \times [0,T], \tag{4.2}$$

where the viscosity coefficient μ is a constant and positive value and a period boundary condition is assumed in this case. The computational domain $[a, b]$ is divided into two subdomains. The left subdomain $[x_{1/2}, x_{J+1/2}]$ is for the DDG methods and the right $[x_{J+1/2}, x_{N+1/2}]$ is for the central difference schemes, where the opposite position would not affect the analysis. The coupling artificial interface is located at $x = x_{J+1/2}$. As an example, we analyze the linear stability of the conservative multidomain hybrid third-order DDG and fourth-order CD method by the way of von-Neumann analysis [2]. As the third-order DDG method and fourth-order central difference scheme are linearly stable when they are applied alone, we only need to give the stability analysis of the multidomain hybrid methods at the coupling cells, for example, the cells I_J or I_{J+1} in (3.7). There are two types of the viscous numerical fluxes constructed at the artificial interface, one is the DDG viscous numerical flux and the other is the CD viscous numerical flux. Therefore, we will have two kinds of the conservative hybrid methods for the viscous terms: multidomain hybrid DDG/CD methods with the DDG viscous numerical flux and multidomain hybrid DDG/CD methods with the CD viscous numerical flux. In the following subsections, we will present the stability analysis of these two kinds of conservative hybrid methods respectively.

4.1.1. Conservative multidomain hybrid DDG/CD methods with the DDG flux

Theorem 4.1. *The conservative multidomain hybrid third-order DDG and fourth-order CD method with the DDG flux is linear stable.*

Proof. If the conservative numerical flux at the artificial interface is set with the DDG flux, which means $\widehat{h}^{CD}_{J+1/2} = \widehat{h}^{DDG}_{J+1/2}$, the semi-form of the hybrid methods at the coupling cells can be written as

$$\begin{cases} \dfrac{d}{dt}u^{DDG}_J = \dfrac{1}{\Delta x}\big(\widehat{h}^{DDG}_{J+1/2} - \widehat{h}^{DDG}_{J-1/2}\big), \\ \dfrac{d}{dt}u^{CD}_{J+1} = \dfrac{1}{\Delta x}\big(\widehat{h}^{CD}_{J+3/2} - \widehat{h}^{DDG}_{J+1/2}\big), \end{cases} \tag{4.3}$$

where

$$\begin{cases} \widehat{h}^{CD}_{J+3/2} = -\dfrac{1}{24}h^{CD}_{J+1/2} + \dfrac{26}{24}h^{CD}_{J+3/2} - \dfrac{1}{24}h^{CD}_{J+5/2}, \\ \widehat{h}^{DDG}_{J+1/2} = h_{J+1/2} + \mathcal{O}(\Delta x^3). \end{cases} \tag{4.4}$$

Here, u^{CD}_{J+1} and u^{DDG}_J represents point values for the CD subdomain and cell average values (zero degree of the freedom) for the DDG subdomain, and the semi-discrete form is not listed out for the higher-order degrees of the freedom of the DDG method.

As the third-order DDG method is stable, we only need to analyze the stability of the coupling cell in the CD subdomain

$$\frac{d}{dt}u^{CD}_{J+1} = \frac{1}{\Delta x}\big(\widehat{h}^{CD}_{J+3/2} - \widehat{h}^{DDG}_{J+1/2}\big). \tag{4.5}$$

According to the formula (2.9), the point values u_{J-1}, u_J, which are needed by the viscous flux $\widehat{h}^{CD}_{J+3/2}$ in the DDG subdomain, can be computed by the DDG methods directly. Another viscous numerical flux $\widehat{h}^{DDG}_{J+1/2}$ can be computed according to the three steps in Section 3.1. Finally, we can obtain the viscous numerical flux of the coupling cell I_{J+1} as follows:

$$\begin{cases} \widehat{h}^{CD}_{J+3/2} = \dfrac{\mu}{17280\Delta x}\big(-22710u_{J+1} + 22710u_{J+2} - 1995u_{J+3} + 111u_{J+4} \\ \qquad\qquad -111u^0_{J-1} + 37u^2_{J-1} + 1995u^0_J - 665u^2_J\big), \\ \widehat{h}^{DDG}_{J+1/2} = \dfrac{\mu}{1728\Delta x}\big(3150u_{J+1} - 384u_{J+2} + 51u_{J+3} - 57u^0_{J-1} + 19u^2_{J-1} \\ \qquad\qquad -2760u^0_J - 1728^1_J - 232u^2_J\big), \end{cases} \tag{4.6}$$

where the parameters u^0_{J-1}, u^1_{J-1}, u^2_{J-1} and u^0_J, u^1_J, u^2_J are the degrees of freedom in cells I_{J-1} and I_J in the DDG subdomain, respectively.

The von-Neumann analysis of the FD methods is based on the amplification factor while of which the DG methods is based on the amplification matrix. Therefore, the relationship between the point value and the degree of freedom should be established first. A fifth-order Lagrange interpolation polynomial is constructed to approximate the function $u(x,t)$ in the formula (2.3).

For cell I_J, the fifth-order interpolation polynomial is constructed as

$$p_J(x) = \sum_{k=J}^{J+4} l_k(x)u(x_k), \quad l_k(x) = \prod_{j=J, j\neq k}^{J+4} \frac{x - x_j}{x_k - x_j}. \tag{4.7}$$

Replacing the function $u(x,t)$ with $p_J(x)$, we can obtain the following formulas:

$$\begin{aligned} u^0_J &= \frac{6463}{5760}u_J - \frac{523}{1440}u_{J+1} + \frac{383}{960}u_{J+2} - \frac{283}{1440}u_{J+3} + \frac{223}{5760}u_{J+4}, \\ u^1_J &= -\frac{103}{96}u_J + \frac{169}{80}u_{J+1} - \frac{33}{20}u_{J+2} + \frac{181}{240}u_{J+3} - \frac{23}{160}u_{J+4}, \\ u^2_J &= \frac{493}{1344}u_J - \frac{367}{336}u_{J+1} + \frac{269}{224}u_{J+2} - \frac{199}{336}u_{J+3} + \frac{157}{1344}u_{J+4}. \end{aligned} \tag{4.8}$$

Similarly, the degrees of freedom in cell I_{J-1} can be disposed. Therefore, we can obtain the viscous numerical flux with the point values as follows:

$$\begin{cases} \widehat{h}^{CD}_{J+3/2} = -\dfrac{\mu}{25804800\Delta x}\Big(165723u_{J-1} - 2978387u_J + 33910718u_{J+1} \\ \qquad\qquad -33909462u_{J+2} + 2976503u_{J+3} - 162095u_{J+4}\Big), \\ \widehat{h}^{DDG}_{J+1/2} = -\dfrac{\mu}{860160\Delta x}\Big(28367u_{J-1} + 661052u_J - 376070u_{J+1} \\ \qquad\qquad -541292u_{J+2} + 284911u_{J+3} - 56968u_{J+4}\Big). \end{cases} \tag{4.9}$$

With the first-order Euler forward method in time discretization, we can obtain the final discrete form of the equation in the coupling cell I_{J+1}

$$u^{n+1}_{J+1} = u^n_{J+1} + \frac{\mu\Delta t}{\Delta x^2}\frac{1}{25804800}\Big(685287u^n_{J-1} + 22809947u^n_J$$

$$
\begin{aligned}
&- 45192818u_{J+1}^n + 17670702u_{J+2}^n \\
&+ 5570827u_{J+3}^n - 1543945u_{J+4}^n\Big). \qquad (4.10)
\end{aligned}
$$

In order to calculate the amplification factor, the point values u_j^n, $j = J-1, \ldots, J+4$ can be replaced by the general terms of the Fourier series $v^n \exp(ikx_j)$, $j = J-1, \ldots, J+4$, where the notation i is the imaginary unit. The parameter κ is define as

$$
\kappa = \mu \frac{\Delta t}{\Delta x^2}. \qquad (4.11)
$$

Finally, we can calculate the amplification factor

$$
\begin{aligned}
G = 1 + \frac{\kappa}{25804800\Delta x^2}\Big(&22809947e^{-k\Delta xi} + 17670702e^{k\Delta xi} + 685287e^{-2k\Delta xi} \\
&+ 5570827e^{2k\Delta xi} - 1543945e^{3k\Delta xi} - 45192818\Big). \qquad (4.12)
\end{aligned}
$$

To estimate the absolute value of amplification factor, we can further simplify the value G in the form of the $\mathrm{Real} + \mathrm{Imag} * i$, where the notation Real and Imag are the real and imaginary part of the amplification factor respectively,

$$
\begin{aligned}
\mathrm{Real} &= 1 + \kappa\Big(- \frac{1429137}{716800} + \frac{11278121\cos(k\Delta x)}{6451200} + \frac{3128057\cos^2(k\Delta x)}{6451200} \\
&\qquad - \frac{308789\cos^3(k\Delta x)}{1290240}\Big), \qquad (4.13) \\
\mathrm{Imag} &= -\kappa \frac{1027849\sin(k\Delta x) - 977108\sin(2k\Delta x) + 308789\sin(3k\Delta x)}{5160960}.
\end{aligned}
$$

After a series of trigonometric transformations, we can calculate the final stability condition with respect to $|G| \leq 1$

$$
0 < \kappa \leq 0.998. \qquad (4.14)
$$

According to the von-Neumann analysis, the conservative multidomain hybrid third-order DDG and fourth-order CD method with the DDG flux is linear stable under the condition of $0 < \kappa \leq 0.998$. The detailed estimation of the parameter κ is given in the Appendix. □

4.1.2. Conservative multidomain hybrid DDG/CD methods with the CD flux

Theorem 4.2. *The conservative multidomain hybrid third-order DDG and fourth-order CD method with the CD flux is linear stable.*

Proof. If the conservative numerical flux at the artificial interface is set with the CD flux, which means $\widehat{h}_{J+1/2}^{DDG} = \widehat{h}_{J+1/2}^{CD}$, the equations of the multidomain hybrid methods

at the coupling cells can be written as

$$\begin{cases} \dfrac{d}{dt}u_J^{DDG} = \dfrac{1}{\Delta x_J}\big(\widehat{h}_{J+1/2}^{CD} - \widehat{h}_{J-1/2}^{DDG}\big), \\ \dfrac{d}{dt}u_{J+1}^{CD} = \dfrac{1}{\Delta x_{J+1}}\big(\widehat{h}_{J+3/2}^{CD} - \widehat{h}_{J+1/2}^{CD}\big). \end{cases} \tag{4.15}$$

Similarly, we need to analyze the stability of the coupling cell I_J in the DDG subdomain and the complete forms of the equation are

$$\begin{cases} \dfrac{d}{dt}u_J^0 = \dfrac{1}{\Delta x}\big(\widehat{h}_{J+1/2}^{CD} - \widehat{h}_{J-1/2}^{DDG}\big), \\ \dfrac{d}{dt}u_J^1 = \dfrac{3}{\Delta x}\big(\widehat{h}_{J+1/2}^{CD} + \widehat{h}_{J-1/2}^{DDG}\big) - \dfrac{6}{\Delta x^2}\displaystyle\int_{I_J} u_x dx, \\ \dfrac{d}{dt}u_J^2 = \dfrac{15}{2\Delta x}\big(\widehat{h}_{J+1/2}^{CD} - \widehat{h}_{J-1/2}^{DDG}\big) - \dfrac{90}{\Delta x^3}\displaystyle\int_{I_J} u_x(x - x_J)dx. \end{cases} \tag{4.16}$$

According to the multidomain hybrid methods, we can obtain the viscous numerical flux in the above equations as follows:

$$\begin{aligned} \widehat{h}_{J+1/2}^{CD} = \frac{1}{17280\Delta x}\Big(&22710u_{J+1} - 1995u_{J+2} + 111u_{J+3} - 111u_{J-2}^0 + 37u_{J-2}^2 \\ &+ 1995u_{J-1}^0 - 665u_{J-1}^2 - 22710u_J^0 + 7570u_J^2\Big), \\ \widehat{h}_{J-1/2}^{DDG} = \frac{1}{3\Delta x}\Big(&3u_{J-1}^1 + 4u_{J-1}^2 + 3u_J^1 - 4u_J^2 - 6\Delta x u_{J-1}^0 - 6\Delta x u_{J-1}^1 \\ &- 4\Delta x u_{J-1}^2 + 6\Delta x u_J^0 - 6\Delta x u_J^1 + 4\Delta x u_J^2\Big), \end{aligned} \tag{4.17}$$

where the parameters u_k^0, u_k^1, u_k^2 $(k = J-2, J-1, J)$ are the degrees of freedom in the cell k, and the fifth-order Lagrange interpolation polynomials can be applied just like Eq. (4.7).

As for the integral terms in the Eq. (4.16), the direct derivative of the respective fifth-order Lagrange interpolation polynomials are used to approximate the function u_x and the integral terms can be simplified in a similar way. A simple calculation shows that

$$\frac{d}{dt}u^{DDG}\Big|_{x_J} = \frac{d}{dt}u_J^0 - \frac{d}{3dt}u_J^2. \tag{4.18}$$

With the first-order Euler forward method in time discretization, we can obtain the final discrete form of the equation at the coupling cell I_J

$$\begin{aligned} u_J^{n+1} = u_J^n - \frac{\mu\Delta t}{\Delta x^2}\frac{1}{8601600}\Big(&852431u_{J-2} - 11175804u_{J-1} + 19728346u_J \\ &- 9256124u_{J+1} - 231729u_{J+2} + 82880u_{J+3}\Big). \end{aligned} \tag{4.19}$$

After replacing the point values u_j^n, $j = J-2, \ldots, J+3$ with the general terms of the Fourier series $v^n \exp(ikx_j)$, $j = J-2, \ldots, J+3$, we can calculate the amplification

factor G and then separate G into the real part Real and the imaginary part Imag respectively, where

$$\begin{aligned}\mathrm{Real} = 1 + \kappa\Big(&-\frac{4776911}{2150400} + \frac{258507\cos(k\Delta x)}{1075200} - \frac{310351\cos^2(k\Delta x)}{2150400} \\ &- \frac{37\cos^3(k\Delta x)}{960}\Big), \\ \mathrm{Imag} = &-\frac{857\sin(k\Delta x) - 484\sin(2k\Delta x) + 37\sin(3k\Delta x)}{3840}.\end{aligned} \tag{4.20}$$

Finally, we can calculate the final stability condition with respect to $|G| \leq 1$

$$0 < \kappa \leq 0.892. \tag{4.21}$$

According to the von-Neumann analysis, the conservative multidomain hybrid third-order DDG and fourth-order CD method with the CD flux is linear stable under the condition of $0 < \kappa \leq 0.892$. The estimation of the amplification factor G is similar to the Appendix, which is omitted in this paper. □

4.2. Accuracy analysis

In this subsection, we will give the accuracy analysis of the multidomain hybrid methods for the viscous terms.

Theorem 4.3. *The conservative multidomain hybrid DDG/CD methods for the viscous terms is of first-order accuracy.*

Proof. As shown in Fig. 1, we assume that the left subdomain is computed by the k-th order DDG methods and the right subdomain is computed by the central difference schemes and the artificial interface is located at $x = x_{J+1/2}$. Either the CD flux or the DDG flux is taken as the unique numerical flux at $x = x_{J+1/2}$, we can obtain the equation of the conservative hybrid methods at the coupling cell generally

$$\frac{d}{dt}u_J = \frac{1}{\Delta x_J}\big(\widehat{h}^{CD}_{J+1/2} - \widehat{h}^{DDG}_{J-1/2}\big), \tag{4.22}$$

where $\widehat{h}^{CD}_{J+1/2}, \widehat{h}^{DDG}_{J-1/2}$ are the viscous numerical fluxes computed by the central difference schemes and DDG methods at the interfaces $x_{J+1/2}, x_{J-1/2}$ respectively. As for the k-th order DDG flux, the relation with the exact numerical flux at the interface is

$$\widehat{h}^{DDG}_{J-1/2} = h_{J-1/2} + \mathcal{O}(\Delta x^k). \tag{4.23}$$

However, from Shu and Osher [35], we know that the relationship between $h^{CD}_{J+1/2}$ and the exact viscous flux $h_{J+1/2}$ is

$$\widehat{h}^{CD}_{J+1/2} = h_{J+1/2} - \frac{\Delta x^2}{24}\frac{d^2h}{dx^2}\Big|_{x_{J+1/2}} + \mathcal{O}(\Delta x^4). \tag{4.24}$$

It means that the conservative viscous numerical flux computed by the central difference schemes at an interface is lower than the exact numerical flux in the range of $\mathcal{O}(\Delta x^2)$. This leads to the fact that

$$\widehat{h}^{CD}_{J+1/2} - \widehat{h}^{DDG}_{J-1/2} = h_{J+1/2} - h_{J-1/2} + \mathcal{O}(\Delta x^2). \tag{4.25}$$

Thus, with a Δx in the denominator of the form of a semi-discrete scheme, the conservative hybrid multidomain DDG/CD methods for the viscous terms are first-order accuracy. □

Theorem 4.4. *The nonconservative multidomain hybrid third-order DDG and fourth-order CD method for the viscous terms is of third-order accuracy.*

Proof. For the DDG subdomain, the values of the ghost points in the CD subdomain are of fourth-order accuracy, which are higher-order than third-order DDG methods. As for the CD subdomain, the values of the ghost points in the DDG subdomain are only of third-order accuracy, which is the main error in the whole domain. We take the artificial interface located at $x = x_{J+1/2}$ as an example and analyze the accuracy of the coupling cell I_{J+1} in the CD subdomain, which is shown in Fig. 1(b).

To analyze the accuracy of the coupling cell in the CD subdomain, Taylor expansions at the point x_{J+1} can be performed according to the formulas (2.3). The viscous numerical fluxes of the cell I_{J+1} can be calculated as follows:

$$\begin{cases} \widehat{R}^{4thCD}_{J+1/2} = \mu\left(u_x - \dfrac{\Delta x}{2}u_{xx} + \dfrac{\Delta x^2}{12}u_{xxx} + \dfrac{1157\Delta x^3}{4300800}u_{xxxx}\right)\Big|_{x_{J+1}} + \mathcal{O}(\Delta x^4), \\ \widehat{R}^{4thCD}_{J+3/2} = \mu\left(u_x + \dfrac{\Delta x}{2}u_{xx} + \dfrac{\Delta x^2}{12}u_{xxx} - \dfrac{157\Delta x^3}{6451200}u_{xxxx}\right)\Big|_{x_{J+1}} + \mathcal{O}(\Delta x^4). \end{cases} \tag{4.26}$$

Therefore, the semi-discrete form of the coupling cell I_{J+1} can be simplified as

$$\frac{d}{dt}u^{CD}_{J+1} = \frac{\widehat{R}_{J+3/2} - \widehat{R}_{J+1/2}}{\Delta x} = \mu\left(u_{xx} - \frac{757\Delta x^2}{2580480}u_{xxxx}\right)\Big|_{x_{J+1}} + \mathcal{O}(\Delta x^3). \tag{4.27}$$

As can be seen, the accuracy of the coupling cell I_{J+1} is of second-order accuracy, which is one order lower than third-order DDG method. According to the theory of Ref. [17, 18], if the boundary precision is one order lower than the inner cells, the overall accuracy of the solution is kept at the higher order, where the overall third-order accuracy of the whole computational domain can be preserved. □

5. Extension to hyperbolic-parabolic equations

In this section, we mainly focus on the extension of the multidomain hybrid methods to the following hyperbolic-parabolic equation:

$$\begin{cases} u_t + f(u)_x = h(u, u_x)_x, & x \in [a, b], \\ u(x, 0) = u_0(x), & t \in [0, T], \end{cases} \tag{5.1}$$

which is a simplified model equation of the Navier-Stokes equations. The computational domain $[a, b]$ is divided into two subdomains as shown in Fig. 1, where the artificial interface is located at $x = x_{J+1/2}$. Corresponding to the DDG methods for the viscous terms, the DG methods are used to discrete the inviscid terms. Multiplying Eq. (5.1) by the test function $v(x)$, and integrating by parts in I_j, we can obtain the weak form formulation

$$\int_{I_j} u_t v dx + \big(\widehat{f}(u) - \widehat{h}(u, u_x)\big)v\big|_{j-1/2}^{j+1/2} - \int_{I_j} \big(f(u) - h(u, u_x)\big)v_x dx = 0. \tag{5.2}$$

The inviscid numerical fluxes $\widehat{f}(u)_{j\pm1/2}$ are approximated via a numerical flux denoted by $\widehat{f}(u^-, u^+)$, which is a monotone flux and satisfies the Lipschitz continuity condition. The integral $\int_{I_j}(f(u) - h(u, u_x))v_x dx$ can be either computed exactly or approximated by using suitable numerical quadratures. For the Eq. (5.1), the conservative schemes in the finite difference methods can be written as

$$u_t + \frac{\widehat{f}_{j+1/2} - \widehat{f}_{j-1/2}}{\Delta x} = \frac{\widehat{h}_{j+1/2} - \widehat{h}_{j-1/2}}{\Delta x}, \tag{5.3}$$

where the flux $\widehat{f}_{j\pm1/2}$ are the inviscid numerical fluxes, which are disposed by the fifth-order finite difference WENO schemes [19] in this paper to capture the discontinuities.

At the coupling cells I_J, I_{J+1}, the informations needed by the inviscid numerical fluxes $\widehat{f}^{DG}_{J+1/2}$ and $\widehat{f}^{WENO}_{J+1/2}$, which are the values of variable u only, are included in the construction of the multidomain hybrid DDG/CD methods. Therefore, the inviscid numerical fluxes $\widehat{f}^{DG}_{J+1/2}$ and $\widehat{f}^{WENO}_{J+1/2}$ can be calculated in a similar way. For the multidomain hybrid methods, the subdomains computed by the DG methods and the DDG methods are uniformly called the DG subdomains, while the subdomains computed by the finite difference WENO schemes and central difference schemes are called the FD subdomains.

For the extension to two-dimensional Navier-Stokes equations, it is straightforward and with no essential difficulties. More Gauss quadrature points at the artificial interface have to be reconstructed as shown in Fig. 2(b). Finally, we summarize the strategies of the multidomain hybrid methods for the hyperbolic-parabolic equations in the following steps:

Algorithm 5.1

1: Decompose the computational domain.
2: Initialize the degrees of freedom for the DG methods and the point values for the FD methods according to the initial conditions.
3: Assign the values of the ghost points for the FD methods, and then calculate the inviscid numerical flux $\widehat{f}^{WENO}_{j+1/2}$, $j = J, J+1, \ldots, N$ and the viscous numerical flux $\widehat{h}^{CD}_{j+1/2}$, $j = J, J+1, \ldots, N$ in the FD subdomains.

4: Calculate the inviscid numerical flux $\widehat{f}^{DG}_{j+1/2}$, $j = 0, 1, \ldots, J-1$ and the viscous numerical flux $\widehat{h}^{DDG}_{j+1/2}$, $j = 0, 1, \ldots, J-1$ in the DG subdomains except the artificial interfaces.
5: Use a shock detector to detect the possible discontinuity at the artificial interface: If the coupling cell does not include discontinuity, then the nonconservative hybrid methods are adopted. Otherwise, the conservative hybrid methods are applied with a unique conservative numerical flux at the artificial interface.
6: If the nonconservative hybrid methods are applied at the coupling cells, construct the Lagrange interpolation polynomials for the DG subdomains, calculate the first and second derivatives needed by the DG methods, compute the inviscid numerical flux $\widehat{f}^{DG}_{J+1/2}$ and the viscous numerical flux $\widehat{h}^{DDG}_{J+1/2}$ at the artificial interface.
7: Update the degrees of freedom in the DG subdomains and the point values in the FD subdomains respectively.
8: Advance to the next moment according to the third-order SSPRK method and repeat the Steps 3-7 until to the given calculation time.

6. Numerical results

In this section, we will demonstrate the performance of the multidomain hybrid methods for the viscous flow problems.

6.1. Accuracy test

Example 6.1. We solve a linear diffusion equation with the following initial and periodic boundary condition:

$$\begin{cases} u_t = u_{xx}, \\ u(x,0) = \cos(x), \quad -\pi \le x \le \pi, \end{cases} \tag{6.1}$$

where the exact solution of this problem is $u(x,t) = e^{-t}\cos(x)$. We simply decompose $[-\pi, \pi]$ into three parts: the boundary subdomains $[-\pi, 0.5\pi]$ and $[0.5\pi, \pi]$ and the inner subdomain $[-0.5\pi, 0.5\pi]$. The DDG methods are applied in the boundary subdomains, while the central difference schemes are in the inner subdomain. The computational time is till to 1.0. To test the accuracy and the stability of the different conservative viscous numerical fluxes, the DDG flux is chosen at the artificial interface $x = -0.5\pi$ and the CD flux is chosen at $x = 0.5\pi$. The respective errors and the convergence rates of the conservative multidomain hybrid DDG and CD method are shown in Table 5. The numerical results verify the theoretical analysis of Theorems 4.1-4.3, where both of the conservative viscous flux are stable and a second-order accuracy can be observed in this case.

Table 5: Accuracy for the conservative multidomain hybrid 3rd-DDG and 4th-CD method (Example 6.1).

N	$L_1-error$	order	$L_2-error$	order	$L_\infty-error$	order
24	1.291e-03		1.340e-03		2.027e-03	
48	3.231e-04	1.998	3.347e-04	2.001	5.068e-04	2.000
96	8.079e-05	1.999	8.366e-05	2.000	1.265e-04	2.002
192	2.020e-05	1.999	2.091e-05	2.000	3.160e-05	2.001
384	5.050e-06	1.999	5.228e-06	2.000	7.896e-06	2.000

Example 6.2. Next, we solve a linear diffusion equation with the following initial and periodic boundary condition:

$$\begin{cases} u_t = u_{xx}, \\ u(x,0) = \sin(x), \quad 0 \le x \le 2\pi, \end{cases} \tag{6.2}$$

where the exact solution of this problem is $u(x,t) = e^{-t}\sin(x)$.

The decomposition of the domain is the same with Example 6.1 and the computational time is till to 1.0. Numerical results calculated by the nonconservative hybrid DDG and CD method are shown in Table 6, where a third-order accuracy can be observed and it agrees well with Theorem 4.4.

Table 6: Accuracy for the nonconservative multidomain hybrid 3rd-DDG and 4th-CD method (Example 6.2).

N	$L_1-error$	order	$L_2-error$	order	$L_\infty-error$	order
24	7.330e-05		9.253e-05		1.763e-04	
48	8.823e-06	3.054	1.146e-05	3.013	2.196e-05	3.004
96	1.078e-06	3.032	1.422e-06	3.010	2.750e-06	2.997
192	1.329e-07	3.019	1.770e-07	3.006	3.437e-07	3.000
384	1.649e-08	3.011	2.207e-08	3.003	4.295e-08	3.000

Example 6.3. Here, we solve a linear convection-diffusion equation with the following initial and periodic boundary condition:

$$\begin{cases} u_t + u_x = \mu u_{xx}, \\ u(x,0) = \dfrac{1}{4} + \dfrac{1}{2}\sin(\pi x), \quad x \in [-1,1], \end{cases} \tag{6.3}$$

where the exact solution is

$$u(x,t) = \frac{1}{4} + \frac{1}{2}e^{-\mu\pi^2 t}\sin\big(\pi(x-t)\big).$$

The parameter μ is taken as 0.1 and the computational time is till to 1.0. The boundary subdomains $[-1.0,-0.5]$ and $[0.5,1.0]$ are computed by the third-order DG and third-order DDG methods, while the inner subdomain $[-0.5,0.5]$ are computed by the fifth-order WENO and fourth-order CD schemes. For the consideration of the stability, the

Table 7: Accuracy for the conservative multidomain hybrid method (Example 6.3).

N	$L_1 - error$	order	$L_2 - error$	order	$L_\infty - error$	order
24	3.338e-04		3.998e-04		7.036e-04	
48	7.316e-05	2.189	8.230e-05	2.280	1.319e-04	2.414
96	1.821e-05	2.006	2.039e-05	2.012	3.230e-05	2.030
192	4.565e-06	1.996	5.107e-06	1.997	8.156e-06	1.985
384	1.143e-06	1.997	1.278e-06	1.998	2.044e-06	1.996

Table 8: Accuracy for the third-order nonconservative hybrid methods (Example 6.3).

N	$L_1 - error$	order	$L_2 - error$	order	$L_\infty - error$	order
24	1.660e-04		2.029e-04		3.925e-04	
48	6.038e-06	4.781	6.921e-06	4.874	1.315e-05	4.898
96	4.257e-07	3.826	5.603e-07	3.626	1.121e-06	3.552
192	5.598e-08	2.926	7.570e-08	2.887	1.488e-07	2.914
384	7.272e-09	2.944	9.652e-09	2.971	1.878e-08	2.985

DG and DDG numerical fluxes are taken as the unique fluxes at the artificial interface $x = -0.5$, while the WENO and CD numerical fluxes are taken as the unique fluxes at the artificial interface $x = 0.5$.

The results of the conservative and nonconservative multidomain hybrid methods are shown in Tables 7 and 8 respectively, which agree well with the analysis of the accuracy in Theorems 4.3 and 4.4 and the expected second-order and third-order accuracy can be observed in this case.

Example 6.4. In this example, we consider the two-dimensional linear convection-diffusion equation

$$u_t + u_x + u_y = \epsilon(u_{xx} + u_{yy}), \quad (x, y) \in [0, 2\pi]^2 \tag{6.4}$$

with $\epsilon = 0.5$ and the initial condition

$$u(x, y, t = 0) = \sin(x)\sin(y).$$

The exact solution of this problem is

$$u(x, y, t) = \exp(-t)\sin(x - t)\sin(y - t)$$

cf. [1]. The computational domain is decomposed into two parts: the left part $[0, \pi] * [0, 2\pi]$ and the right part $[\pi, 2\pi] * [0, 2\pi]$. The third-order DG and DDG methods are applied in the left part, while the fifth-order WENO and fourth-order CD schemes are in the right part. In Table 9, we give the respective errors and convergence rates by the multidomain hybrid methods, and an expected third-order accuracy can be observed in this case.

Table 9: Accuracy for the third-order multidomain hybrid method for 2D linear equation (Example 6.4).

N	$L_1 - error$	order	$L_2 - error$	order	$L_\infty - error$	order
100	2.701e-03		3.255e-03		7.906e-03	
400	1.733e-04	3.962	2.204e-04	3.884	5.845e-04	3.757
1600	1.895e-05	3.193	2.741e-05	3.007	6.592e-05	3.184
6400	2.365e-06	3.002	3.604e-06	2.927	7.863e-06	3.067
25600	3.083e-07	2.939	4.714e-07	2.934	9.793e-07	3.005

Example 6.5. In this example, the compressible Couette flow problem is considered to verify the accuracy and convergence of the multidomain hybrid method for solving the compressible Navier-Stokes equations. Assuming that the viscosity coefficient μ is constant, the analytic solution is given by

$$\begin{aligned} &u = \frac{y}{H}U, \quad v = 0, \quad p = p_\infty, \quad \rho = \frac{p}{RT}, \\ &T = T_0 + \frac{y}{H}(T_1 - T_0) + \frac{y}{H}\left(1.0 - \frac{y}{H}\right)(\gamma - 1)\frac{P_r M_a^2}{2}, \end{aligned} \tag{6.5}$$

where P_r is the Prandtl number, T_0 is a fixed temperature of the bottom plate, T_1 is fixed temperature of the top plate with the moving speed U, H is the distance of the two plates.

In this case, we take $H = 2$, $T_0 = 0.8$, $T_1 = 0.85$ and $P_r = 0.72$. The Mach number for the upper wall $M_a = 0.2$ and the Reynolds number $R_e = 100$ with a constant viscosity coefficient $\mu = 1.0$. The computational domain is a rectangle $(0 \le x \le 2H$ and $0 \le y \le H)$.

The computational domain is decomposed into two subdomains: the left subdomain $(0 \le x \le H, 0 \le y \le H)$ and the right subdomain $(H \le x \le 2H, 0 \le y \le H)$. The respective errors and the convergence rates of the multidomain hybrid methods are shown in Table 10, where an expected third-order accuracy of the norms $L_1, L_2, L_{\inf}$ can be observed.

Table 10: Accuracy for the third-order multidomain hybrid method for the Couette flow (Example 6.5).

N	$L_1 - error$	order	$L_2 - error$	order	$L_\infty - error$	order
50	2.671e-07		3.640e-07		8.779e-07	
200	2.844e-08	3.231	3.976e-08	3.197	1.084e-07	3.017
800	3.276e-09	3.117	4.531e-09	3.133	1.338e-08	3.018
3200	3.830e-10	3.096	5.122e-10	3.144	1.669e-09	3.003
12800	5.249e-11	2.867	6.470e-11	2.985	2.204e-10	2.920

6.2. One-dimensional problems

Example 6.6. Next, we consider the well-known quasi-linear parabolic equation introduced by Burgers [3]

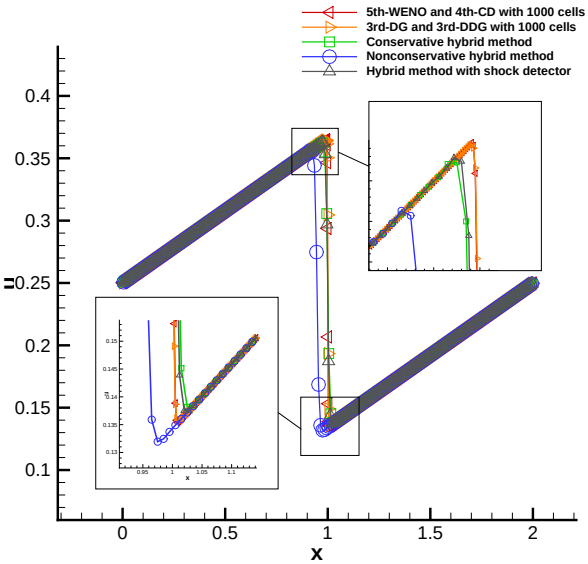

Figure 3: The comparison among the multidomain hybrid methods with $N = 1000$ at $t = 8.0$ (Example 6.6).

$$u_t + uu_x = \nu u_{xx}, \quad x \in [0, 2], \tag{6.6}$$

where ν is a nominally small positive parameter. It is well-known that the nonlinear term in Burgers' equation will cause an initially smooth disturbance to steepen up into a narrow region, which will result in a weak shock problem. Therefore, the notation ν is taken as 0.0001 here to test the ability of capturing the shock waves of the multidomain hybrid methods. The initial condition is

$$u(x, 0) = \frac{1}{4} + \frac{1}{2}\sin(\pi x)$$

and the periodic boundary conditions are considered in this example. The boundary subdomains $[0, 0.6], [1.4, 2]$ are calculated by the third-order DG and DDG methods, while the other subdomains are computed by the fifth-order WENO and fourth-order CD schemes. The results computed by the DG methods and the FD methods with $N = 1000$ are taken as the reference solutions. Numerical results computed by the purely nonconservative and conservative multidomain hybrid methods and the multidomain hybrid methods with a TVB shock detector are shown in Fig. 3, which demonstrate the fact that the multidomain hybrid methods can preserve the high-order accuracy in the smooth regions and the correct position of the shock waves if there is a discontinuity passing through the artificial interface.

Example 6.7. In this example, we consider the one-dimensional scalar convection-diffusion Buckley-Leverett equation introduced in [21]

$$u_t + f(u)_x = \epsilon(\nu(u)u_x)_x, \quad \epsilon\nu(u) \geq 0. \tag{6.7}$$

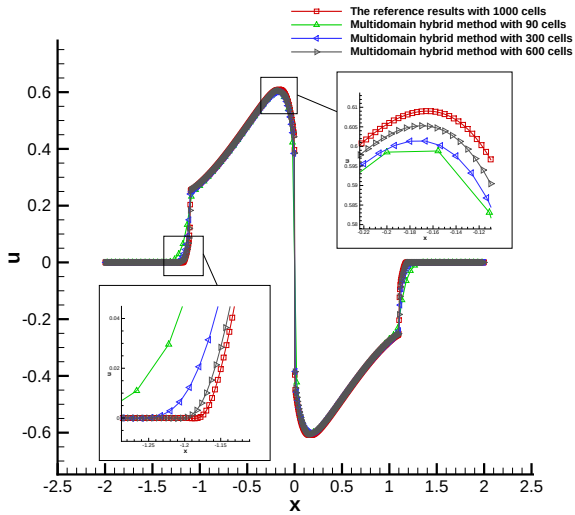

Figure 4: The grid convergence of one-dimensional Buckley-Leverett equation at $t = 0.7$ (Example 6.7).

This is a prototype model for the oil reservoir simulations (two-phases flow). It is an example of strongly degenerate parabolic (or hyperbolic-parabolic) convection-diffusion equation. Considering $\epsilon = 0.1$, $f(u) = u^2$, and

$$\nu(u) = \begin{cases} 0, & |u| \leq 0.25, \\ 1, & |u| > 0.25, \end{cases} \tag{6.8}$$

the variable $\nu(u)$ is discontinuous and therefore the equation is hyperbolic when $u \in [-0.25, 0.25]$ and parabolic elsewhere. We apply the multidomain hybrid methods to this equation subject to the initial condition

$$u(x,0) = \begin{cases} 1, & -1/\sqrt{2} - 0.4 < x < -1/\sqrt{2} + 0.4, \\ -1, & 1/\sqrt{2} - 0.4 < x < 1/\sqrt{2} + 0.4, \\ 0, & \text{otherwise}. \end{cases} \tag{6.9}$$

The computational domain $[-2, 2]$ is decomposed into three parts and the artificial interfaces are set at $x = \pm 4/3$. With the TVB shock detector, the numerical results calculated by the third-order multidomain hybrid method with different cells are shown in Fig. 4. The accurate transition between the hyperbolic and parabolic regions can be observed in the results. With the grid refinement, the numerical results converge to the reference values computed by the fifth-order WENO and fourth-order CD schemes with $N = 1000$.

Example 6.8. Now we consider the Buckley-Leverett equation (6.7) with $\epsilon = 0.01$. The flux function $f(u)$ without gravitational effects

$$f(u) = \frac{u^2}{u^2 + (1-u)^2}$$

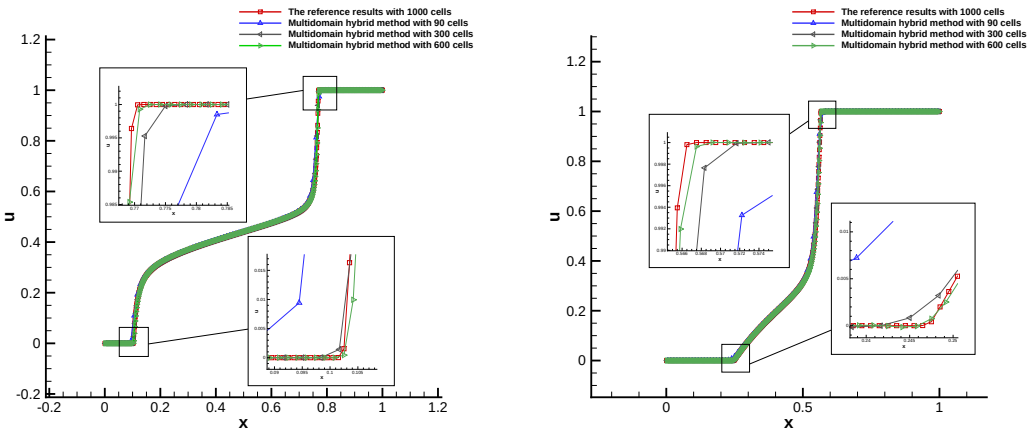

(a) The numerical results without gravitation

(b) The numerical results with gravitation

Figure 5: The grid convergence of one-dimensional Buckley-Leverett equation at $t = 0.2$ (Example 6.8).

and with gravitational effects

$$f(u) = \frac{u^2}{u^2 + (1-u)^2}\big(1 - 5(1-u)^2\big)$$

are both considered in this example. The diffusion coefficient $\nu(u)$ is defined as $\nu(u) = 4u(1-u)$. The initial function is

$$u(x,0) = \begin{cases} 0, & 0 \le x < 1 - 1/\sqrt{2}, \\ 1, & 1 - 1/\sqrt{2} \le x \le 1, \end{cases} \tag{6.10}$$

and the boundary conditions are $u(0,t) = 0.0$ and $u(1,t) = 1.0$. The computational domain is divided into three parts, where the boundary subdomains are calculated by the DG and DDG methods and other subdomains are calculated by the WENO and CD schemes. The artificial interfaces are set at $x = 1/6$ and $x = 5/6$. The numerical results are shown in Fig. 5. With the grid refinement, the numerical results computed by the third-order multidomain hybrid method can converge to the reference values computed by the third-order DG and DDG methods with $N = 1000$.

6.3. Two-dimensional problems

Example 6.9. Next, we solve the following two-dimensional Buckley-Leverett equation [21]:

$$u_t + f(u)_x + g(u)_y = \epsilon(u_{xx} + u_{yy}), \quad (x,y) \in [-1.5, 1.5]^2 \tag{6.11}$$

with $\epsilon = 0.01$ and the flux functions

$$\begin{cases} f(u) = \dfrac{u^2}{u^2 + (1-u)^2}, \\ g(u) = f(u)\big(1 - 5(1-u)^2\big). \end{cases} \tag{6.12}$$

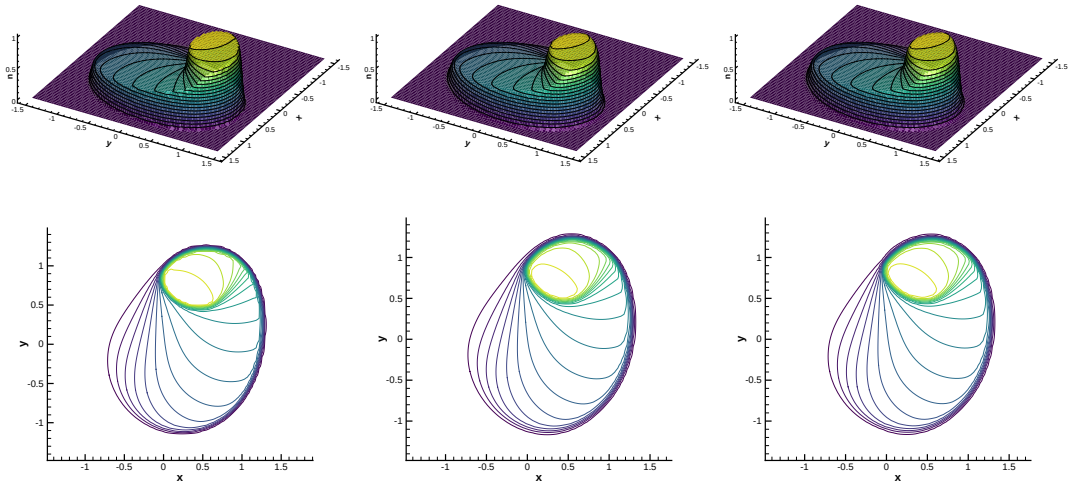

Figure 6: The comparison of the solutions computed by different methods with $N = 80 * 80$ at $t = 0.5$. From left to right: 3rd-DG and 3rd-DDG method, 5th-WENO and 4th-CD method, 3rd-multidomain hybrid method. From top to bottom: two-dimensional Buckley–Leverett equation, 19 contour lines of the solution (Example 6.9).

The initial function for this example is

$$u(x, y, t = 0) = \begin{cases} 1, & x^2 + y^2 < 0.5, \\ 0, & \text{otherwise.} \end{cases} \tag{6.13}$$

As can be seen, gravitational effects are considered in the y-direction in this example. The computational domain is decomposed into two parts, where the left part $[-1.5, 0] * [-1.5, 1.5]$ is computed by DG methods and the right part is computed by the FD methods. The numerical results are shown in Fig. 6, where the results computed by the third-order multidomain hybrid methods compare well with the DG methods and FD methods purely and the results given in [21].

Example 6.10. In this example, we solve the nonlinear and non-degenerate convection-diffusion problem [21]

$$u_t + \left(u - (u - 0.25)^3\right)_x - (u + u^2)_y = \epsilon(u_{xx} + u_{yy}), \quad (x, y) \in [-4, 4]^2 \tag{6.14}$$

with $\epsilon = 0.1$. The initial condition is

$$u(x, y, t = 0) = \begin{cases} 1, & (x - 0.25)^2 + (y - 0.25)^2 < 5, \\ 0, & \text{otherwise.} \end{cases}$$

The computational domain is decomposed into two parts, where the left part $[-4, 0] * [-4, 4]$ is computed by the DG methods and the right part is computed by the FD methods. Numerical results are shown in Fig. 7, where the results computed by the

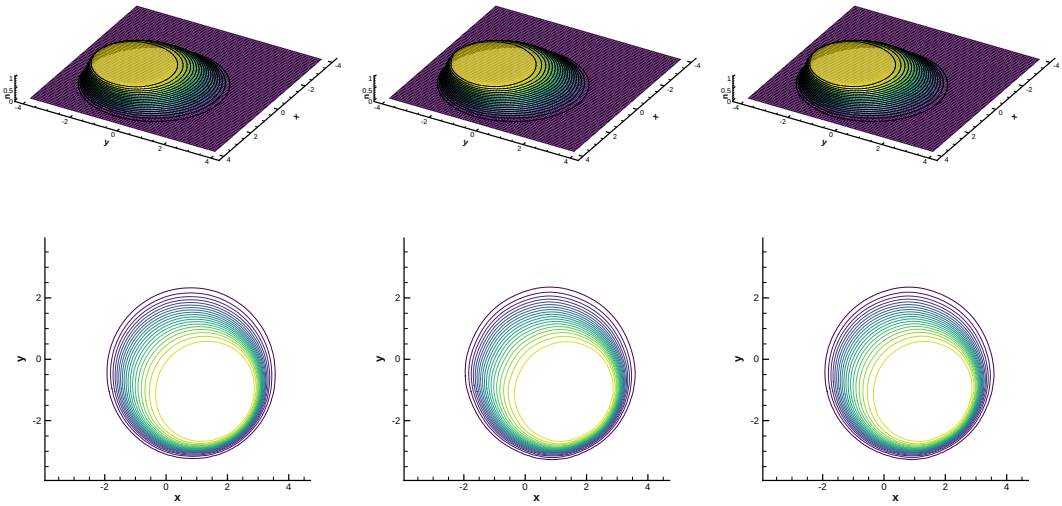

Figure 7: The comparison of the solutions computed by different methods with $N = 80 * 80$ at $t = 0.5$. From left to right: 3rd-DG and 3rd-DDG method, 5th-WENO and 4th-CD method, 3rd-multidomain hybrid method. From top to bottom: the nonlinear and non-degenerate convection-diffusion problem, 19 contour lines of the solution (Example 6.10).

third-order multidomain hybrid methods compare well with the DG methods and FD methods purely and the results given in [21].

Example 6.11 (Viscous Shock Tube Problem)**.** In this example, we consider a two-dimensional viscous shock tube problem [14], which is designed for evaluating different numerical methods for the Navier-Stokes equations. This is a time-dependent unsteady problem. A unit side $([0,1] * [0,1])$ length square shock tube with insulated walls is considered in this example. The diaphragm is initially located in the middle of the tube $x = 0.5$, where the initial condition of the left diaphragm: $\rho_L = 120, u_L = v_L = 0, p_L = \rho_L/\gamma$, and of the right disphragm: $\rho_R = 120, u_R = v_R = 0, p_R = \rho_R/\gamma$.

At the initial time, the diaphragm is broken and a shock wave, followed by a contact discontinuity, moves to the right zone with Mach number $M_a = 2.37$ and reflects at the right end wall. The Prandtl number is 0.72 and a Reynolds number $R_e = 1000$ is considered. The no-slip and adiabatic solid wall conditions are imposed for all boundaries. The computational time is till to $t = 1.0$.

The computational domain is decomposed into two subdomains, where the left subdomain $[0, 0.5] * [0, 1]$ is computed by the DG methods while the other subdomain is for the FD methods. The TVB shock detector is used in this example. With the mesh size $\Delta x = \Delta y = 1/500$, the comparison and the distribution along the line $y = 0.001$ of the density ρ computed by the DG methods, FD methods and multidomain hybrid methods are shown in Figs. 8 and 9 respectively. The flow structure is complicated and the primary vortex calculated by the multidomain hybrid methods are comparable well with the DG methods and FD methods purely.

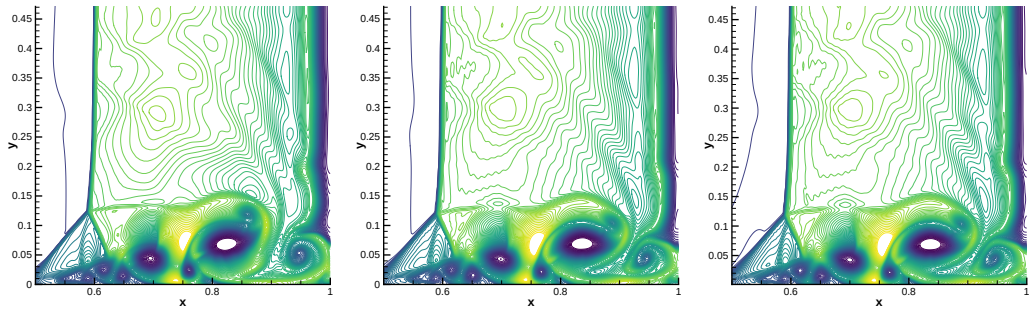

Figure 8: The comparison of the density ρ of viscous shock tube problem at $t = 1$ with $N = 500 * 500$. From left to right: 3rd-DG and 3rd-DDG method, 5th-WENO and 4th-CD method, 3rd-multidomain hybrid method (Example 6.11).

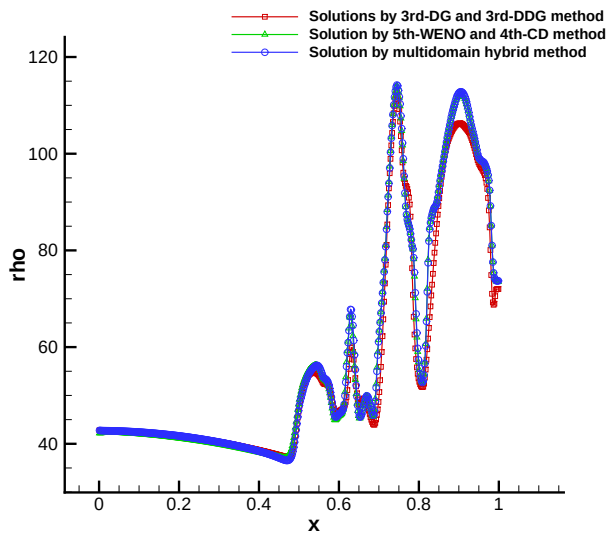

Figure 9: The distribution of the density of viscous shock tube problem along the line $y = 0.001$ (Example 6.11).

Example 6.12 (Shock Layer Interaction Problem [39])**.** A two-dimensional shock layer interaction problem is considered in this example. The problem is designed to focus on the properties of the numerical schemes rather than the boundary treatment in the simulation of the Navier-Stokes equations. An oblique shock from the top left hand corner is made to impact on a spatially developing mixing layer at an initial convective Mach number of 0.6 and is reflected by a wall at the lower boundary. The computational domain is $[0, 200] * [-20, 20]$. The inlet condition at $x = 0$ is specified with a hyperbolic tangent profile

$$u = 2.5 + 0.5 \tanh(2y). \tag{6.15}$$

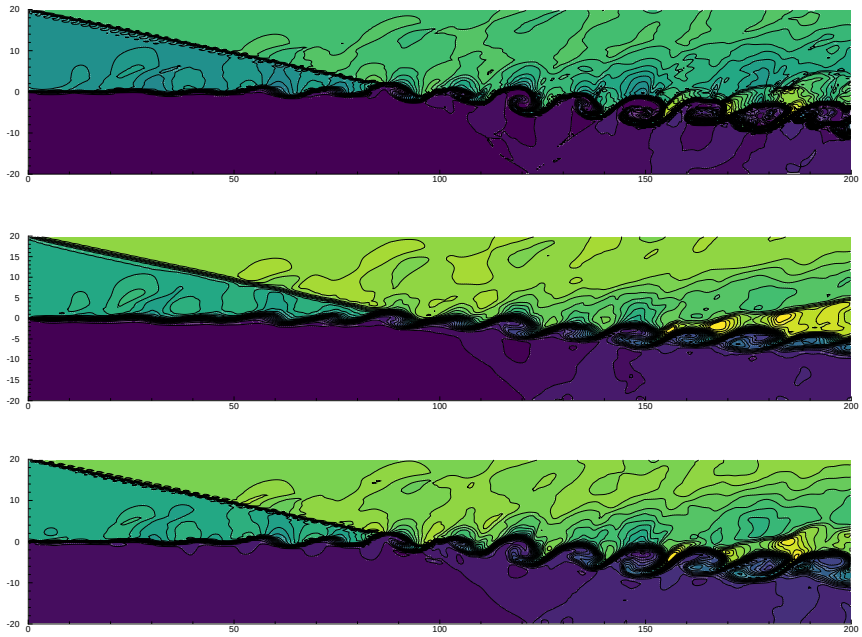

Figure 10: The comparison of the density ρ of the shock layer interaction problem at $t = 120$ with $N = 400 * 80$. From top to bottom: 3rd-DG and 3rd-DDG method, 5th-WENO and 4th-CD method, 3rd-multidomain hybrid method (Example 6.12).

For the upper stream $(y > 0)$, $\rho = 1.6374$, $p = 0.3327$ and for the lower stream $(y < 0)$, $\rho = 0.3626$, $p = 0.3327$. For the upper boundary condition, $u = 2.9709$, $v = -0.1367$, $\rho = 2.1101$, $p = 0.4754$ are taken from the flow properties to make an oblique shock. Fluctuations are added to the inflow as

$$\begin{aligned} \nu' &= \sum_{k=1}^{2} a_k \cos(2\pi k t/T + \phi_k) \exp(-y^2/b), \\ b &= 10, \quad a_1 = a_2 = 0.05, \quad \phi_1 = 0, \quad \phi_2 = \pi/2, \end{aligned} \tag{6.16}$$

where $T = \lambda/u_c$ is period with wavelength $\lambda = 30$, convective velocity $u_c = 2.68$. The Prandtl number Pr is set as 0.72 and the Reynolds number Re is taken as 500. The computational domain is divided decomposed into two subdomains, where the left one $[0, 100]*[-20, 20]$ is calculated by the DG methods and the right one $[100, 200]*[-20, 20]$ is computed by the FD methods with the artificial interface located at $x = 100$. The comparison of the density ρ and the pressure p computed by the DG methods, FD methods and the multidomain hybrid methods are presented in Figs. 10 and 11 respectively. All the methods can capture the shock waves properly and the vortex evolutions in Figs. 10 and 11 are almost indistinguishable. The vortex structures induced by shear layer instabilities can be captured well by the multidomain hybrid methods, which are comparable with the DG methods and FD methods.

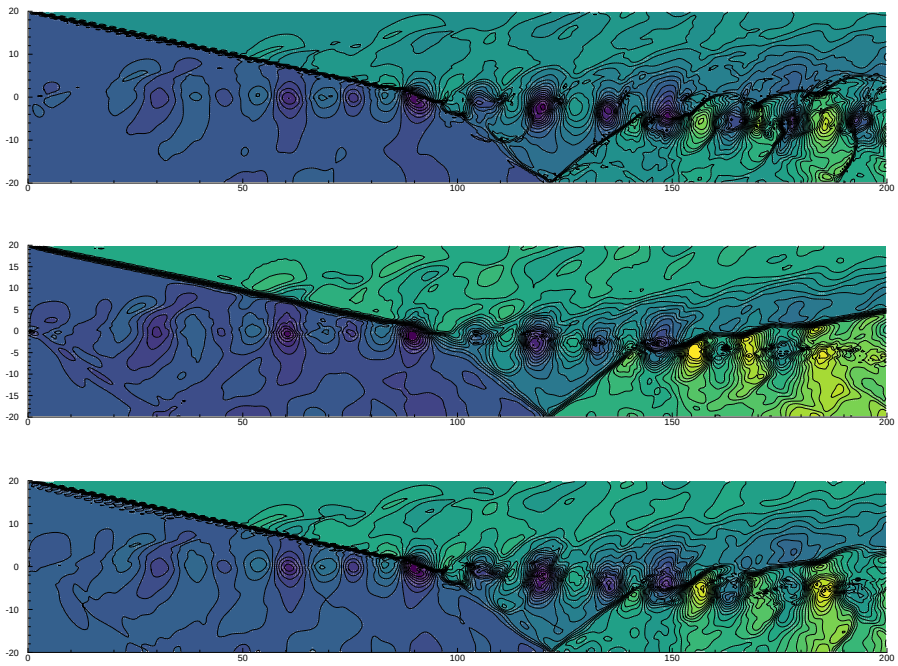

Figure 11: The comparison of the pressure p of the shock layer interaction problem at $t = 120$ with $N = 400 * 80$. From top to bottom: 3rd-DG and 3rd-DDG method, 5th-WENO and 4th-CD method, 3rd-multidomain hybrid method (Example 6.12).

Example 6.13 (Efficiency Comparison)**.** In this example, we give the comparison of the computational efficiency among the fifth-order WENO and fourth-order CD schemes, the third-order DG and DDG methods, and our third-order multidomain hybrid method for solving the two-dimensional viscous shock tube problem in Example 6.11. For the multidomain hybrid methods, we test the different percents of the total meshes near the left boundary wall. All of the computations are executed on the workstation with the Intel(R) Xeon(R) CPU E5-2698 v4 @ 2.20GHz.

The comparison of the computational cost and the computational results are shown in Table 11 and Fig. 12 respectively. With different percents of the total meshes for the DG methods, the computational results compare well with the DG methods and FD methods purely. As can be seen, the third-order DG and DDG methods take the most computational time and the fifth-order WENO and fourth-order CD schemes have the highest efficiency among these methods in this example. The last column in Table 11 denotes the percent of saving computational time compared to the DG method. With the lower percent of the DG subdomain, the computational cost is more close to the FD methods and faster than the DG methods. Specially, with the 4% of the total meshes for DG methods, the third-order multidomain hybrid methods save almost 92.45% time compared to the third-order DG method, which reveals that our multidomain hybrid methods is more highly efficient than the traditional DG methods.

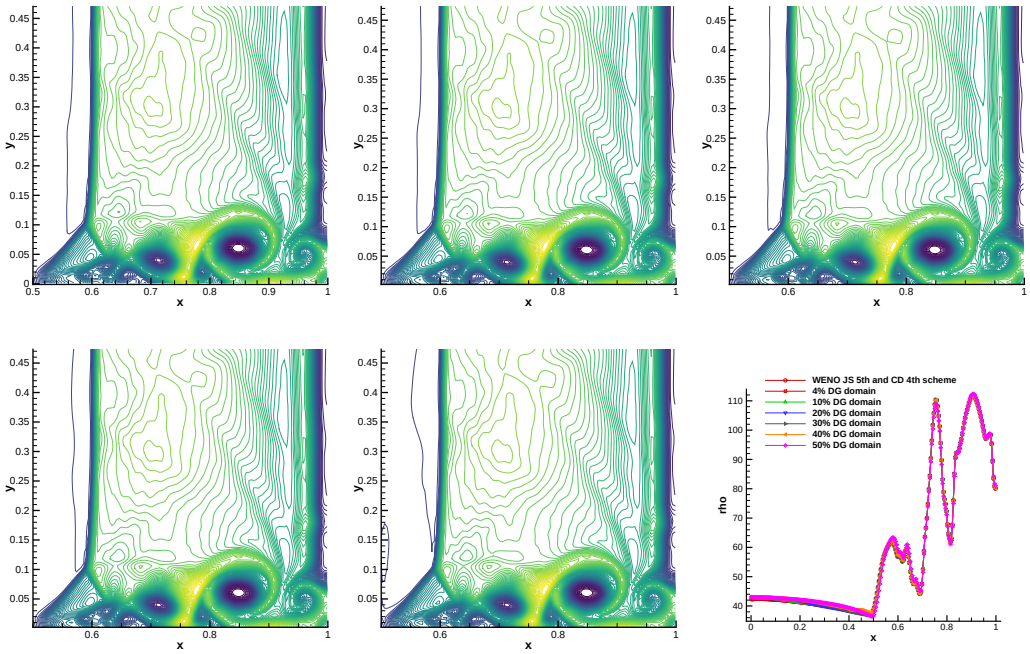

Figure 12: The comparison of the density ρ with different percent of DG domain at $t = 1$ with $N = 250*250$. From left to right and from top to bottom: density with 4% DG, density with 10% DG, density with 20% DG, density with 30% DG, density with 40% DG, density along the line $y = 0.002$ (Example 6.13).

Table 11: The efficiency comparison among the different methods (Example 6.13).

Method	Grid	CFL	CPU time(s)	Percent(%)
5th-WENO and 4th-CD schemes	250*250	0.05	563	96.61
multidomain hybrid method(4%)	250*250	0.05	1252	92.45
multidomain hybrid method(10%)	250*250	0.05	2199	86.74
multidomain hybrid method(20%)	250*250	0.05	3762	77.32
multidomain hybrid method(30%)	250*250	0.05	5355	67.72
multidomain hybrid method(40%)	250*250	0.05	6924	58.26
multidomain hybrid method(50%)	250*250	0.05	8600	48.16
3rd-DG and 3rd-DDG methods	250*250	0.05	16591	-

7. Conclusions

In this paper, we developed two versions of the multidomain hybrid DDG/CD methods for the viscous terms. One is the conservative multidomain hybrid third-order DDG and fourth-order CD method, and the other is the nonconservative multidomain hybrid third-order DDG and fourth-order CD method. Special treatments are used to preserve the conservative property when discontinuities pass through the artificial interfaces and high-order accuracy for smooth regions as well. The analysis of the stability showed

that both the conservative viscous numerical fluxes are linearly stable. Combining with the multidomain hybrid RKDG and WENO methods for the inviscid terms, we extended the multidomain hybrid methods to the hyperbolic-parabolic equations such as two-dimensional Navier-Stokes equations. Numerical results showed that the multidomain hybrid methods can preserve non-oscillation property, high-order accuracy and high efficiency. Further researches to unstructure grids to deal with the complex geometries are ongoing.

Appendix A

In this appendix, we will give the detailed estimation of the amplification factor G in Theorem 4.1. The real and imaginary parts of the amplification factor G are

$$\begin{aligned}\mathrm{Real} = 1+\kappa\Big(&-\frac{1429137}{716800}+\frac{11278121\cos(k\Delta x)}{6451200}+\frac{3128057\cos^2(k\Delta x)}{6451200}\\ &-\frac{308789\cos^3(k\Delta x)}{1290240}\Big),\\ \mathrm{Imag} = -\kappa&\frac{1027849\sin(k\Delta x)-977108\sin(2k\Delta x)+308789\sin(3k\Delta x)}{5160960}.\end{aligned} \tag{A.1}$$

In order to satisfy the stability condition of von-Neumann analysis, it demands that $|G|\le 1$. Moreover, we have $0\le G^2\le 1$. Firstly, we should transform the trigonometric functions to the unified form by the trigonometric formulas

$$\begin{aligned}&\cos(k\Delta x)=\sqrt{1-\sin^2(k\Delta x)},\\ &\cos^2(k\Delta x)=1-\sin^2(k\Delta x),\\ &\cos^3(k\Delta x)=\big(1-\sin^2(k\Delta x)\big)^{3/2},\\ &\sin(2k\Delta x)=2\sin(k\Delta x)\sqrt{1-\sin^2(k\Delta x)},\\ &\sin(3k\Delta x)=3\sin(k\Delta x)-4\sin^3(k\Delta x).\end{aligned} \tag{A.2}$$

Then, two functions $g(x)$ and $f(x)$ are defined as

$$\begin{aligned}g(x)&=\frac{308789}{1290240}x^3-\frac{244277}{645120}x+\frac{244277}{645120}x(1-x^2)^{1/2},\\ f(x)&=-\frac{308789}{1290240}(1-x^2)^{3/2}+\frac{3128057}{6451200}(1-x^2)\\ &\quad+\frac{11278121}{6451200}(1-x^2)^{1/2}-\frac{1429137}{716800},\end{aligned} \tag{A.3}$$

where the definitional domain is $x\in[-1,1]$ and x is real. Therefore, we have

$$G^2=G^2(x)=\big(1+f(x)\kappa\big)^2+\big(g(x)\kappa\big)^2,\quad x\in[-1,1]. \tag{A.4}$$

Simplifying the Eq. (A.4) by notation κ and uniting the similar terms, we can obtain a quadratic function of notation κ

$$G^2(x) = a(x)\kappa^2 + b(x)\kappa + 1, \quad x \in [-1, 1], \tag{A.5}$$

where

$$\begin{aligned} a(x) = &\Bigg(-\frac{3410608278072863}{9007199254740992}x + \frac{3410608278072863}{9007199254740992}x\sigma_1(x) \\ &\quad + \frac{2155664101773481}{9007199254740992}x^3 \Bigg)^2 \\ &+ \Bigg(\sigma_1(x)\sigma_2(x) - \frac{8734819158974251}{18014398509481984}x^2 \\ &\quad + \frac{11278121}{6451200}\sigma_1(x) - \frac{27181815108109389}{18014398509481984} \Bigg)^2, \end{aligned} \tag{A.6}$$

$$\begin{aligned} b(x) = &\, 2\sigma_1(x)\sigma_2(x) - \frac{8734819158974251}{9007199254740992}x^2 + \frac{11278121}{3225600}\sigma_1(x) \\ &- \frac{27181815108109389}{9007199254740992}, \end{aligned}$$

$$\sigma_1(x) = (1 - x^2)^{1/2}, \quad \sigma_2(x) = \frac{2155664101773481}{9007199254740992}x^2 - \frac{2155664101773481}{9007199254740992}.$$

The function $a(x)$ is bigger than zero for $\forall x \in [-1, 1]$. For the inequality equation $0 \leq G^2$, the criterion Δ of the quadratic function is always lower than zero for $\forall x \in [-1, 1]$. As a consequence, the inequality equation $0 \leq G^2$ is always true for κ.

As for the inequality equation $G^2 \leq 1$, the equation can be simplified as

$$a(x)\kappa^2 + b(x)\kappa \leq 0, \quad x \in [-1, 1]. \tag{A.7}$$

Obviously, $\kappa = 0$ is a solution of the inequality equation. With $\kappa > 0$, we have

$$a(x)\kappa \leq -b(x), \quad x \in [-1, 1]. \tag{A.8}$$

Taking $q(x) = -b(x)/a(x)$ and letting its derivative $q_x(x) = 0$, the extreme points can be calculated as

$$x_0 = 0, \quad x_1 = -0.384, \quad x_2 = -0.00207, \quad x_3 = 0.384, \quad x_4 = 0.00207. \tag{A.9}$$

Finally, we take the minimum value among the extreme points and the boundary points and have

$$0 < \kappa \leq 0.998. \tag{A.10}$$

Acknowledgments

The authors would like to thank the anonymous referees for their valuable suggestions.

This work was supported by the National Natural Science Foundation of China (Grant No. 12001031).

References

[1] R. Abedian, H. Adibi, and M. Dehghan, *A high-order weighted essentially non-oscillatory (WENO) finite difference scheme for nonlinear degenerate parabolic equations*, Comput. Phys. Commun. 184 (2013), 1874–1888.

[2] J. D. Anderson and J. Wendt, *Computational Fluid Dynamics*, Vol. 206, Springer, 1995.

[3] E. R. Benton, *Solutions illustrating the decay of dissipation layers in Burgers' nonlinear diffusion equation*, Phys. Fluids 10 (1967), 2113–2119.

[4] J. Cheng and T. Liu, *A multi-domain hybrid DG and WENO method for hyperbolic conservation laws on hybrid meshes*, Commun. Comput. Phys. 16 (2014), 1116–1134.

[5] J. Cheng, X. Liu, T. Liu, and H. Luo, *A parallel, high-order direct discontinuous Galerkin method for the Navier-Stokes equations on 3D hybrid grids*, Commun. Comput. Phys. 21 (2017), 1231–1257.

[6] J. Cheng, Y. Lu, and T. Liu, *Multidomain hybrid RKDG and WENO methods for hyperbolic conservation laws*, SIAM J. Sci. Comput. 35 (2013), A1049–A1072.

[7] J. Cheng, K. Wang, and T. Liu, *A general high-order multi-domain hybrid DG/WENO-FD method for hyperbolic conservation laws*, J. Comput. Math. 34 (2016), 30–48.

[8] J. Cheng, X. Yang, X. Liu, T. Liu, and H. Luo, *A direct discontinuous Galerkin method for the compressible Navier–Stokes equations on arbitrary grids*, J. Comput. Phys. 327 (2016), 484–502.

[9] B. Cockburn, S. Hou, and C.-W. Shu, *The Runge-Kutta local projection discontinuous Galerkin finite element method for conservation laws. IV. The multidimensional case*, Math. Comp. 54 (1990), 545–581.

[10] B. Cockburn, S.-Y. Lin, and C.-W. Shu, *TVB Runge-Kutta local projection discontinuous Galerkin finite element method for conservation laws. III. One-dimensional systems*, J. Comput. Phys. 84 (1989), 90–113.

[11] B. Cockburn and C.-W. Shu, *TVB Runge-Kutta local projection discontinuous Galerkin finite element method for conservation laws. II. General framework*, Math. Comp. 52 (1989), 411–435.

[12] B. Cockburn and C.-W. Shu, *The Runge-Kutta local projection-discontinuous-Galerkin finite element method for scalar conservation laws*, ESAIM: M2AN 25 (1991), 337–361.

[13] B. Cockburn and C.-W. Shu, *The Runge-Kutta discontinuous Galerkin method for conservation laws V: Multidimensional systems*, J. Comput. Phys. 141 (1998), 199–224.

[14] V. Daru and C. Tenaud, *Numerical simulation of the viscous shock tube problem by using a high resolution monotonicity-preserving scheme*, Comput. & Fluids, 38 (2009), 664–676.

[15] S. De Rango and D. Zingg, *Aerodynamic computations using a higher-order algorithm*, in: 37th Aerospace Sciences Meeting and Exhibit, 1999, p. 167.

[16] J. Guo, H. Zhu, Z. Yan, L. Tang, and S. Song, *High-order hybrid WCNS-CPR scheme for shock capturing of conservation laws*, Int. J. Aerosp. Eng. 2020 (2020), 1–13.

[17] B. Gustafsson, *The convergence rate for difference approximations to mixed initial boundary value problems*, Math. Comp. 29 (1975), 396–406.

[18] B. Gustafsson, *The convergence rate for difference approximations to general mixed initial-boundary value problems*, SIAM J. Numer. Anal. 18 (1981), 179–190.

[19] G.-S. Jiang and C.-W. Shu, *Efficient implementation of weighted ENO schemes*, J. Comput. Phys. 126 (1996), 202–228.

[20] Y. Jiang, *High order finite difference multi-resolution weno method for nonlinear degenerate parabolic equations*, J. Sci. Comput. 86 (2021), 1–20.

[21] A. Kurganov and E. Tadmor, *New high-resolution central schemes for nonlinear conser-*

vation laws and convection-diffusion equations, J. Comput. Phys. 160 (2000), 241–282.

[22] H. LIU AND J. YAN, *The direct discontinuous Galerkin (DDG) methods for diffusion problems*, SIAM J. Numer. Anal. 47 (2009), 675–698.

[23] H. LIU AND J. YAN, *The direct discontinuous Galerkin (DDG) method for diffusion with interface corrections*, Commun. Comput. Phys. 8 (2010), p. 541.

[24] H. LUO, L. LUO, AND R. NOURGALIEV, *A reconstructed discontinuous Galerkin method for the Euler equations on arbitrary grids*, Commun. Comput. Phys. 12 (2012), 1495–1519.

[25] V. MALTSEV, D. YUAN, K. W. JENKINS, M. SKOTE, AND P. TSOUTSANIS, *Hybrid discontinuous Galerkin-finite volume techniques for compressible flows on unstructured meshes*, J. Comput. Phys. 473 (2023), p. 111755.

[26] W. H. REED AND T. R. HILL, *Triangular mesh methods for the neutron transport equation*, Tech. Rep., Los Alamos Scientific Lab., N. Mex.(USA), 1973.

[27] Y. SHEN, B. WANG, AND G. ZHA, *Implicit WENO scheme and high order viscous formulas for compressible flows*, in: 25th AIAA Applied Aerodynamics Conference, 2007, p. 4431.

[28] Y. SHEN AND G. ZHA, *Large eddy simulation using a new set of sixth order schemes for compressible viscous terms*, J. Comput. Phys. 229 (2010), 8296–8312.

[29] Y. SHEN, G. ZHA, AND X. CHEN, *High order conservative differencing for viscous terms and the application to vortex-induced vibration flows*, J. Comput. Phys. 228 (2009), 8283–8300.

[30] Y. SHEN, G. ZHA, AND B. WANG, *Large eddy simulation of circular cylinder flow by using higher order WENO schemes*, in: 38th Fluid Dynamics Conference and Exhibit, 2008, p. 3748.

[31] C.-W. SHU, *Essentially non-oscillatory and weighted essentially non-oscillatory schemes for hyperbolic conservation laws. In: Advanced Numerical Approximation of Nonlinear Hyperbolic Equations. Lecture Notes in Mathematics*, Vol. 1697, Springer, (1998), 325–432.

[32] C.-W. SHU ET AL., *Different formulations of the discontinuous Galerkin method for the viscous terms. In: Advances in Scientific Computing*, Science Press (2001), 144–155.

[33] C.-W. SHU AND S. OSHER, *Efficient implementation of essentially non-oscillatory shock-capturing schemes*, J. Comput. Phys. 77 (1988), 439–471.

[34] C.-W. SHU AND S. OSHER, *Efficient implementation of essentially non-oscillatory shock-capturing schemes, II*, J. Comput. Phys. 83 (1989), 32–78.

[35] C.-W. SHU AND S. OSHER, *Efficient implementation of essentially non-oscillatory shock-capturing schemes, II*, Springer, 1997.

[36] R. J. SPITERI AND S. J. RUUTH, *A new class of optimal high-order strong-stability-preserving time discretization methods*, SIAM J. Numer. Anal. 40 (2002), 469–491.

[37] K. WANG, J. CHENG, AND T. LIU, *High order finite difference scheme based on DG boundary treatment (FDbDG)*, Commun. Comput. Phys. 25 (2019), 1413–1445.

[38] Z. WANG, J. ZHU, Y. YANG, AND N. ZHAO, *A new fifth-order alternative finite difference multi-resolution WENO scheme for solving compressible flow*, Comput. Methods Appl. Mech. Engrg. 382 (2021), p. 113853.

[39] H. C. YEE, N. D. SANDHAM, AND M. J. DJOMEHRI, *Low-dissipative high-order shock-capturing methods using characteristic-based filters*, J. Comput. Phys. 150 (1999), 199–238.

[40] F. ZHANG, J. CHENG, AND T. LIU, *A direct discontinuous Galerkin method for the incompressible Navier-Stokes equations on arbitrary grids*, J. Comput. Phys. 380 (2019), 269–294.

[41] F. ZHANG, T. LIU, AND J. CHENG, *High order stable multi-domain hybrid RKDG and WENO-FD methods*, J. Comput. Math. 36 (2018), p. 517.

[42] L. Zhang, W. Liu, L. He, and X. Deng, *A class of hybrid DG/FV methods for conservation laws III: Two-dimensional Euler equations*, Commun. Comput. Phys. 12 (2012), 284–314.
[43] L. Zhang, W. Liu, M. Li, X. He, and H. Zhang, *A class of DG/FV hybrid schemes for conservation law IV: 2D viscous flows and implicit algorithm for steady cases*, Comput. & Fluids 97 (2014), 110–125.
[44] L. Zhang, L. Wei, H. Lixin, D. Xiaogang, and Z. Hanxin, *A class of hybrid DG/FV methods for conservation laws I: Basic formulation and one-dimensional systems*, J. Comput. Phys. 231 (2012), 1081–1103.
[45] L. Zhang, L. Wei, H. Lixin, D. Xiaogang, and Z. Hanxin, *A class of hybrid DG/FV methods for conservation laws II: Two-dimensional cases*, J. Comput. Phys. 231 (2012), 1104–1120.
[46] M. Zhao, X. Wang, X. Li, Z. Liu, W. Liu, and K. Yang, *A hierarchical reconstruction for DG/FV method with low dispersion: Basic formulation and applications*, Comput. & Fluids 231 (2021), p. 105175.
[47] H. Zhu, Z. Yan, H. Liu, M. Mao, and X. Deng, *High-order hybrid WCNS-CPR schemes on hybrid meshes with curved edges for conservation laws I: Spatial accuracy and geometric conservation laws*, Commun. Comput. Phys. 23 (2018), 1355–1392.
[48] J. Zhu and C.-W. Shu, *A new type of multi-resolution weno schemes with increasingly higher order of accuracy on triangular meshes*, J. Comput. Phys. 392 (2019), 19–33.
[49] D. Zingg, S. De Rango, M. Nemec, and T. Pulliam, *Comparison of several spatial discretizations for the Navier-Stokes equations*, J. Comput. Phys. 160 (2000), 683–704.